The American Journal of Pathology, Vol. 184, No. 9, September 2014

The American Journal of
PATHOLOGY
ajp.amjpathol.org

ANIMAL MODELS

Retinal and Nonocular Abnormalities in *Cyp27a1*$^{-/-}$ *Cyp46a1*$^{-/-}$ Mice with Dysfunctional Metabolism of Cholesterol

Aicha Saadane,* Natalia Mast,* Casey D. Charvet,* Saida Omarova,* Wenchao Zheng,* Suber S. Huang,*† Timothy S. Kern,‡ Neal S. Peachey,§¶‖ and Irina A. Pikuleva*

From the Departments of Ophthalmology and Visual Sciences and Medicine,‡ Case Western Reserve University and University Hospitals,† Cleveland; the Department of Ophthalmology,‖ Cleveland Clinic Lerner College of Medicine, Case Western Reserve University, Cleveland; the Cole Eye Institute,§ Cleveland Clinic Foundation, Cleveland; and the Cleveland VA Medical Center,¶ Cleveland, Ohio*

Accepted for publication May 29, 2014.

Address correspondence to Irina A. Pikuleva, Ph.D., Department of Ophthalmology and Visual Sciences, Case Western Reserve University, 2085 Adelbert Rd, Room 303a, Cleveland, OH 44106. E-mail: iap8@case.edu.

Cholesterol elimination from nonhepatic cells involves metabolism to side-chain oxysterols, which serve as transport forms of cholesterol and bioactive molecules modulating a variety of cellular processes. Cholesterol metabolism is tissue specific, and its significance has not yet been established for the retina, where cytochromes P450 (CYP27A1 and CYP46A1) are the major cholesterol-metabolizing enzymes. We generated *Cyp27a1*$^{-/-}$*Cyp46a1*$^{-/-}$ mice, which were lean and had normal serum cholesterol and glucose levels. These animals, however, had changes in the retinal vasculature, retina, and several nonocular organs (lungs, liver, and spleen). Changes in the retinal vasculature included structural abnormalities (retinal-choroidal anastomoses, arteriovenous shunts, increased permeability, dilation, nonperfusion, and capillary degeneration) and cholesterol deposition and oxidation in the vascular wall, which also exhibited increased adhesion of leukocytes and activation of the complement pathway. Changes in the retina included increased content of cholesterol and its metabolite, cholestanol, which were focally deposited at the apical and basal sides of the retinal pigment epithelium. Retinal macrophages of *Cyp27a1*$^{-/-}$*Cyp46a1*$^{-/-}$ mice were activated, and oxidative stress was noted in their photoreceptor inner segments. Our findings demonstrate the importance of retinal cholesterol metabolism for maintenance of the normal retina, and suggest new targets for diseases affecting the retinal vasculature. *(Am J Pathol 2014, 184: 2403–2419; http://dx.doi.org/10.1016/j.ajpath.2014.05.024)*

Cholesterol maintenance in the retina is still poorly understood, perhaps because of cellular and laminar complexity of the retina and unique functions related to phototransduction and transmission of the visual signal.[1,2] The sources of retinal cholesterol have been established, however, and include local synthesis as well as uptake from the systemic circulation across the blood-retina barrier.[3–5] The mechanisms for cholesterol elimination have also been elucidated, and involve lipoprotein-mediated transport[1] and enzymatic processing by different cytochrome P450 (CYP) enzymes.[6–12] The daily process of photoreceptor (PR) phagocytosis represents an additional pathway of retinal cholesterol removal.[13] Nevertheless, the quantitative significance, coordination, and role of the different pathways for retinal cholesterol input and output remain unclear.

We focused on CYP27A1 and CYP46A1 because these enzymes are responsible for most of the cholesterol metabolism in the retina.[8–11] Both use cholesterol as a substrate but generate different products: 27-hydroxycholesterol and 5-cholestanoic acid (CYP27A1) or 24S-hydroxycholesterol

Supported in part by NIH grant EY018383 (I.A.P.), Visual Sciences Training Program predoctoral research training fellowship T32 EY07157 (C.D.C), Visual Sciences Research Center Core Facility grant P30 EY11373, Ohio Lions Eye Research Foundation funds, VA funds, Foundation Fighting Blindness funds, Research to Prevent Blindness unrestricted grants, and the Jules and Doris Stein Professorship from the Research to Prevent Blindness Foundation (I.A.P.).

Disclosures: None declared.

Current address of S.O., Department of Family Medicine, Wexner Medical Center, the Ohio State University, Columbus, OH.

http://dx.doi.org/10.1016/j.ajpath.2014.05.024

(CYP46A1).[10] Hydroxylation makes cholesterol more soluble and, thus, able to spontaneously diffuse out of cells into the circulation.[14] Accordingly, side-chain oxysterols represent the forms of cholesterol in which excess tissue cholesterol is transported to the liver for further degradation to bile acids. In addition, 27-hydroxycholesterol, 5-cholestanoic acid, and 24S-hydroxycholesterol could play regulatory roles by interacting with different proteins. Oxysterols can bind to the insulin-induced gene protein and 3-hydroxy-3-methyl-glutaryl-CoA reductase and thereby regulate cholesterol biosynthesis.[15] Oxysterols can also activate transcription factors of the liver X receptor (LXR) family[16–18] and thereby control cholesterol removal by lipoproteins. Collectively, through interactions with different proteins, oxysterols couple three pathways of cellular cholesterol homeostasis: cholesterol biosynthesis, cholesterol metabolism, and elimination by lipoproteins. In addition, by activating LXRs, oxysterols participate in the regulation of fatty acid and triglyceride biosynthesis, glucose metabolism, and immune-inflammatory responses.[17,19] The affinity of oxysterols for LXRs depends on their structure, and LXR-mediated gene activation is tissue and gene specific.[20–22]

We recently reported that mice lacking CYP27A1 develop retinal-choroidal anastomoses (RCAs) characteristic of age-related macular degeneration (AMD) type 3, and that these lesions are associated with focal cholesterol-containing deposits along Bruch's membrane.[12] Herein, we generated mice that lack both CYP27A1 and CYP46A1. CYP27A1 is found in almost every cell in the retina and is highly expressed in the inner segments (ISs), Müller cells, and retinal pigment epithelium (RPE).[6,13] Retinal distribution of CYP46A1 is more restricted and limited to the ganglion cell layer (GCL), inner plexiform–inner nuclear layer (INL) interface, and the RPE.[7,13,23] Outside the retina, CYP27A1 is ubiquitous and particularly abundant in the liver, vascular endothelium, and macrophages, especially lung macrophages.[24–27] Nonocular expression of CYP46A1 is limited to the brain,[28] where CYP46A1 is present at levels approximately 7× higher than those in the retina.[9] We hypothesized that the retina may have a more severe phenotype than that of *Cyp27a1*$^{-/-}$ mice if both CYP27A1 and CYP46A1 were ablated, because this model would have a greater impact on retinal cholesterol metabolism and the production of the regulatory side-chain oxysterols. The latter could be particularly important: in addition to oxysterols produced intracellularly, each retinal cell type is exposed to oxysterols generated by other cell types, and may uptake these preformed oxysterols during their diffusion to the intraretinal and choroidal vascular networks that supply blood to the inner and outer retina, respectively. Endothelial cells of the intraretinal capillaries do not have circular openings (fenestrae) in their wall and are exposed to a slower rate of blood flow compared with choroidal vessels, which have fenestrae that face the retina. Hence, retina-generated oxysterols probably have a slower diffusion rate across the wall of the intraretinal capillaries than of the choriocapillaris. Coupled with high expression of CYP27A1 in vascular endothelium,[25] these peculiarities of the retina suggest that retinal vasculature is exposed to relatively high levels of oxysterols and should be sensitive to the lack of oxysterol production. Consistent with our expectations, a wide variety of retinal vascular lesions were found in *Cyp27a1*$^{-/-}$*Cyp46a1*$^{-/-}$ mice, with some being similar to those characteristic of type 3 neovascular AMD and some typical of early-stage diabetic retinopathy. As reported herein, the retina, as well as some nonocular organs, cannot compensate for a simultaneous lack of CYP27A1 and CYP46A1, and develops pathological features that reflect the tissue response to cholesterol overload and impaired oxysterol production. The present work expands our knowledge of retinal abnormalities associated with disturbed cholesterol metabolism, and suggests that molecules mimicking a regulatory function of oxysterols (namely, agonists of LXRs) should be considered for the treatment of AMD and diabetic retinopathy.

Materials and Methods

Animals

Cyp27a1$^{+/-}$ mice on the C57BL/6J background[29] and *Cyp46a1*$^{-/-}$ mice on the mixed C57BL/6J;129S6/SvEv background[30] were obtained from the laboratory of Dr. Sandra Erickson (University of California, San Francisco, San Francisco, CA) and Dr. David Russell (University of Texas Southwestern, Dallas, TX), respectively. These animals were bred to generate *Cyp27a1*$^{-/-}$*Cyp46a1*$^{-/-}$ line and *Cyp27a1*$^{+/+}$ *Cyp46a1*$^{+/+}$ littermates. F_5 and subsequent generations of *Cyp27a1*$^{-/-}$*Cyp46a1*$^{-/-}$ and *Cyp27a1*$^{+/+}$*Cyp46a1*$^{+/+}$ mice were used for all experiments. Animals were aged 3 to 6 months, unless otherwise indicated. Mice were maintained on a standard 12-hour light (approximately 10 lux)–dark cycle and were fed standard rodent chow and water ad libitum. All animal procedures were approved by the Case Western Reserve University (Cleveland, OH) Institutional Animal Care and Use Committee and conformed to recommendations of the American Veterinary Association Panel on Euthanasia and the Association for Research in Vision and Ophthalmology.

Sterol Quantifications

Mice were anesthetized with 80 mg/kg ketamine and 15 mg/kg xylazine in phosphate-buffered saline (PBS) and sacrificed by cervical dislocation. The eyes were enucleated, the anterior segment was removed, and the lens with the vitreous humor was squeezed out of the eye cup. The retina/RPE was carefully scooped with a microspatula and dipped quickly 3× in PBS. Samples of the washed retina/RPE from 40 animals of the same sex and genotype were combined, and the pooled sample was homogenized as described.[10] The homogenate was divided into three portions, each processed separately for sterol content determination by isotope dilution gas chromatography–mass spectrometry, as

described.[10] The analyses were conducted separately in males and females. The analyses used unsaponified retinal extracts as sterols, mainly unesterified in the retina, and some of them (eg, pregnenolone and 7-ketocholesterol) decompose during the saponification step needed to measure total (unesterified plus esterified) sterol content.[10] Cholesterol was the only sterol for which unesterified and total amounts were measured. The measurements of cholestanol were based on [$^2H_4$]lathosterol as internal standard and used the 215 *m/z* ion for cholestanol and 259 *m/z* ion for [$^2H_4$] lathosterol.

Retinal Imaging and Function

Ultra–high-resolution spectral-domain optical coherence tomography (SD-OCT), fluorescein angiography (FA), transmission electron microscopy (TEM), and electroretinographic (ERG) recordings were as described.[12,31] We used the 840HHP SD-OCT system (Bioptigen, Durham, NC), a scanning laser ophthalmoscope (Spectralis HRA+OCT; Heidelberg Engineering, Carlsbad, CA), a 1200EX transmission electron microscope (JEOL Ltd, Peabody, MA), and a Universal Testing and Electrophysiological System UTAS E-3000 (LKC Technologies Inc., Gaithersburg, MD), respectively. For electroretinography, mice were dark adapted overnight and then anesthetized with 80 mg/kg ketamine and 15 mg/kg xylazine in PBS via i.p. injection. The pupils were dilated with 1% tropicamide eye drops. ERGs were recorded using a contact lens electrode placed on each cornea. Needle electrodes placed in the scalp and tail were used as reference and ground, respectively. White strobe flashes were presented to the dark-adapted eye in order of increasing stimulus strength (from −3.7 to 2.1 log cd·s/m^2). At each stimulus level, three to five responses were averaged, and interstimulus intervals ranged from 10 seconds to 1 minute for the highest flash stimuli. After 7 minutes of adaptation to a steady background (150 cd/m^2), light-adapted, cone-mediated ERGs were recorded in response to strobe stimuli superimposed on the background. The a-wave amplitude was measured at 7 milliseconds after flash presentation from the prestimulus baseline. The amplitude of the b-wave was measured from the a-wave minimum to the b-wave maximum.

The preparation of retinal and aortic root sections, flat mounts, elastase digests, and histological stains with oil red O, filipin, tomato lectin, and antibodies against iso[4]LGE$_2$ were as previously described.[12,31–33] Immunostaining for iso[4]LGE$_2$ adducts required pretreatment with phospholipase A$_2$ (PLA$_2$) to cleave the carboxylate ester and increase immunoreactivity. This was performed as described[31] by placing retinal sections in 200 U/mL PLA$_2$-containing digest buffer (25 mmol/L Tris-Cl, pH 7.5, containing 10 mmol/L CaCl$_2$, 100 mmol/L KCl, 100 μg/mL butylated hydroxytoluene, and 0.02% Triton X-100) for 1 hour at 37°C. Slides were then washed 3× for 5 minutes in PBS containing 0.05% Tween 20 (PBS-Tween), extracted with 70% ethanol in water for 5 minutes, and washed again 3× with PBS-Tween. Sections were blocked for 1 hour with 5% nonimmunized goat serum (Invitrogen, Grand Island, NY) in PBS-Tween (blocking buffer) and incubated overnight at 4°C with iso[4]LGE$_2$ antiserum or nonimmunized rabbit serum (dilution, 1:2500 in blocking buffer). Next morning, slides were washed 3× for 5 minutes in PBS-Tween and incubated for 1 hour in dark with DyLight 649–conjugated goat anti-rabbit IgG (Jackson ImmunoResearch, West Grove, PA), diluted 1:200 in blocking buffer. Slides were washed 3× with PBS-Tween, then 2× with water, blotted dry, and mounted with ProLong Gold with DAPI (Invitrogen) and a glass coverslip. For other immunostaining, PLA$_2$ digest was omitted and the dilution and source of primary antibodies were 1:1000 for rabbit anti–ionized calcium binding adaptor molecule 1 (Iba1; Wako, Richmond, VA), 1:100 for rat anti-F4/80 (AbDSerotec, Raleigh, NC), 1:200 for mouse anti–7-ketocholesterol (JaICA, Fukuroi, Japan), 1:50 for mouse anti-CD11b (Hycult Biotech, Plymouth Meeting, PA), and 1:50 for mouse anti-complement factors complement protein 3 (C3)/cleavage product 3a (C3a) and C9 (Hycult Biotech). Anti-Iba1 and anti-F4/80 were visualized with goat anti-rabbit DyLight 649 secondary antibodies (Jackson ImmunoResearch) and anti-rat IgG Alexa Fluor 647 (Cell Signaling, Danvers, MA), respectively, used at a 1:200 dilution. The detection of primary antibodies from mice was by the Mouse on Mouse Elite Peroxidase Kit (Vector Laboratories, Burlingame, CA) and used ImmPACT VIP Peroxidase Substrate (Vector Laboratories). Slides were imaged on an inverted microscope (model DMI 6000 B; Leica Microsystems) using a Retiga EXi-Fast camera (QImaging, Surrey, BC, Canada). Histological quantifications of staining with oil red O and antibodies against Iba1, CD11b, complement factors C3/C3a and C9, iso[4]LGE$_2$, and 7-ketocholesterol were performed in Metamorph software (Molecular Devices Corp., Sunnyvale, CA), with an equal area of retinas being examined for all images. Positive staining was identified and recorded as a percentage of the area examined.

PCR Arrays and RT-qPCR

Retinas from four mice per genotype were combined, and total RNA was isolated by the TRIzol Reagent (Life Technologies, Grand Island, NY). Total RNA (1 μg) was then converted to cDNA by SuperScript III Reverse Transcriptase (Invitrogen) and used for gene profiling by the lipoprotein signaling and cholesterol metabolism and angiogenesis PCR arrays (SABiosciences, Valencia, CA). PCR arrays were run in the Mastercycler RealPlex^2 machine (Eppendorf, Hauppauge, NY). Changes between the genotypes in gene expression were calculated, as described,[13] after normalization to the five housekeeping genes (glucuronidase β, hypoxanthine guanine phosphoribosyl transferase 1, heat shock protein 90α class B member, glyceraldehyde-3-phosphate dehydrogenase, and β-actin). Subsequent validation of gene expression by quantitative RT-PCR (RT-qPCR) was performed using the primers that were designed and assessed, as described,[13] with the PCRs

being performed in triplicate and normalized to β-actin. The message levels for *Abcg1* in the lungs were assessed in individual animals ($n = 3$ for *Cyp27a1*$^{-/-}$*Cyp46a1*$^{-/-}$ mice; $n = 4$ for *Cyp27a1*$^{+/+}$*Cyp46a1*$^{+/+}$ littermates) and then averaged.

Measurement of Liver Triglycerides

Lipids from liver homogenates (15%, w/v) were extracted with 19 volumes of chloroform/methanol (2:1, v/v), dried, and saponified overnight in 1N KOH/70% aqueous ethanol at 55°C. Glycerol content was measured after sample neutralization with $MgCl_2$ using the Free Glycerol Reagent kit (Sigma-Aldrich, St. Louis, MO), according to the manufacturer's protocol.

Serum Chemistry and Glucose Tolerance

Blood (5 to 10 μL) was withdrawn from the tail vein of mice fasted overnight and assayed for glucose and hemoglobin A_{1c} levels by an Elite XL Glucometer (Bayer Contour, Whippany, NJ) and VARIANT II kit (Bio-Rad, Hercules, CA), respectively. Serum lipids were measured after overnight fasting as well. Animals were sacrificed, and serum was isolated as described.[34] Total cholesterol, high-density lipoprotein, low-density lipoprotein (LDL), triglycerides, and free fatty acids were measured by Marshfield Labs (Marshfield Clinic, Marshfield, WI). To measure tolerance to glucose, a solution of 50% D-glucose (2 g/kg body weight) was injected i.p., and the blood glucose was determined 10, 20, 30, 60, 90, 120, and 150 minutes after the injection.

Statistical Analysis

All images are representative of studies in three to five animals per genotype. The quantitative data represent means ± SEM; the number of animals (n) is indicated in each figure. Either a two-tailed, unpaired, Student's t-test or the two-way repeated-measures analysis of variance (SAS Institute, Inc., Cary, NC) was used to determine statistical significance, which is defined as $P < 0.05$, $P < 0.01$, and $P < 0.001$. The two-way repeated-measures analysis of variance was applied to the glucose tolerance tests and ERG recordings. The repeated measures were the individual (in the same animal) glucose levels at different time points or individual ERG responses to different intensity of the flash light. When analysis of variance showed major interactions, post hoc contrasts between the same points in different groups were performed using the t-test and then corrected by the Bonferroni test.

Results

Altered Cholesterol Maintenance in the *Cyp27a1*$^{-/-}$ *Cyp46a1*$^{-/-}$ Retina

The levels of cholesterol precursors lanosterol, lathosterol, and desmosterol (Figure 1A) were essentially unchanged in both sexes of *Cyp27a1*$^{-/-}$*Cyp46a1*$^{-/-}$ mice (Figure 1B), with the exception of a slight, but significant, 1.2-fold increase in females for lathosterol, a marker for cholesterol biosynthesis.[35] The cholesterol metabolites and products of CYP27A1 (27-hydroxycholesterol and 5-cholestenoic acid) were not detected in the *Cyp27a1*$^{-/-}$*Cyp46a1*$^{-/-}$ retina (Figure 1C), because they were not detected in the *Cyp27a1*$^{+/+}$*Cyp46a1*$^{+/+}$ retina, where these sterols are lower than the limits of detection (1 pmol/mg protein) and at much lower levels than the levels of 27-hydroxycholesterol and 5-cholestenoic acid in human retina.[10] These interspecies differences could be due to a much shorter death-to-tissue preservation time (<1 hour for mouse retinas and approximately 12 hours for human retinas) preventing sterol accumulation due to arrested blood flow. Alternatively, there may be enzymes in mouse, but not human, retina that act on these products, also reducing the steady-state levels of CYP27A1 metabolites in mice. The product of CYP46A1 (24-hydroxycholesterol) was not detected in the *Cyp27a1*$^{-/-}$ *Cyp46a1*$^{-/-}$ retina (Figure 1C), consistent with the absence of this metabolic pathway. Pregnenolone, a product of CYP11A1, was not detected either. Thus, abolished cholesterol metabolism via CYP27A1 and CYP46A1 was not compensated by either increased metabolism by CYP11A1 or reduction in cholesterol biosynthesis. The levels of unesterified cholesterol (UC) were unchanged in *Cyp27a1*$^{-/-}$ *Cyp46a1*$^{-/-}$ females and were decreased 1.7-fold in males compared with the sex-matched *Cyp27a1*$^{+/+}$*Cyp46a1*$^{+/+}$ littermates (Figure 1D). This could reflect a reduced uptake of blood-borne cholesterol, increased cholesterol elimination via lipoprotein-mediated transport, and/or increased cholesterol esterification to store sterol excess in intracellular lipid droplets. The latter possibility was tested by the measurements of total (unesterified plus esterified) retinal cholesterol. The levels of total cholesterol were increased 1.8- and 2-fold in *Cyp27a1*$^{-/-}$*Cyp46a1*$^{-/-}$ females and males, respectively (Figure 1D), thus indicating that when retinal cholesterol metabolism is abolished, cholesterol is accumulated in the retina and begins to be esterified.

We measured retinal cholestanol, a hallmark sterol accumulating along with cholesterol in the form of xanthomas in tendons and brain of patients with CYP27A1 deficiency.[36] Xanthomas are absent in *Cyp27a1*$^{-/-}$ mice, despite increased sterol levels in the plasma, tendons, and brain.[37] Retinal cholestanol levels were increased 10-fold in *Cyp27a1*$^{-/-}$*Cyp46a1*$^{-/-}$ females and 5-fold in *Cyp27a1*$^{-/-}$ *Cyp46a1*$^{-/-}$ males (Figure 1E), prompting the measurements of cholestanol in the retinas of *Cyp27a1*$^{-/-}$ and *Cyp46a1*$^{-/-}$ mice. In both genotypes, cholestanol was altered only slightly, compared with their wild-type littermates (Figure 1E). Thus, a greater than fivefold increase in cholestanol seems to be a distinct feature of the *Cyp27a1*$^{-/-}$ *Cyp46a1*$^{-/-}$ retina.

We next investigated the distribution of the unesterified retinal sterols by staining with the fluorescent compound filipin interacting with the sterol 3β-hydroxyl group.[38] UC is the

major retinal sterol[39] and the sterol present at approximately eightfold higher levels than unesterified cholestanol in tendon xanthomas in CYP27A1-deficient people.[40] Accordingly, filipin staining in the *Cyp27a1*$^{-/-}$*Cyp46a1*$^{-/-}$ retinas most likely reflects the distribution of UC. Overall, histochemistry with filipin was similar in the *Cyp27a1*$^{-/-}$*Cyp46a1*$^{-/-}$ and *Cyp27a1*$^{+/+}$*Cyp46a1*$^{+/+}$ retinas, except that a distinct fluorescent line was observed in the wall of many intraretinal blood vessels (Figure 2, B and C), suggesting sterol accumulation. In addition, the *Cyp27a1*$^{-/-}$*Cyp46a1*$^{-/-}$ retinas had intense focal fluorescent signals at the apical and basal sides of the RPE (Figure 2, B and C) and labeling of the lumen of some of the choroidal vessels (Figure 2B). Deposits at the basal aspect of the RPE were also detected by TEM (Figure 2E), although their composition was not investigated. Deposit-containing RPE cells had increased granule (either melanosomes or lipofuscin) formation, which could lead to the RPE dysfunction.[41,42]

Finally, we investigated retinal expression of cholesterol-related genes. Only male mice were analyzed, because they had more pronounced changes of total retinal cholesterol than females. We used a PCR array to profile 84 genes from the pathways of cholesterol synthesis, uptake, intracellular processing, trafficking, storage, metabolism, efflux, and regulation (Supplemental Table S1 and Supplemental Figure S1). Of these, only three (*Cyp46a1*, *Akr1d1*, and *Cela3b*) showed a greater than twofold change in expression (an arbitrary cutoff limit) in the *Cyp27a1*$^{-/-}$*Cyp46a1*$^{-/-}$ compared with the *Cyp27a1*$^{+/+}$*Cyp46a1*$^{+/+}$ retina. mRNA levels of cholesterol-esterifying enzymes sterol O-acyltransferase (SOAT)1 and SOAT2 were unaltered, consistent with the primarily translational and post-translational, but not transcriptional,

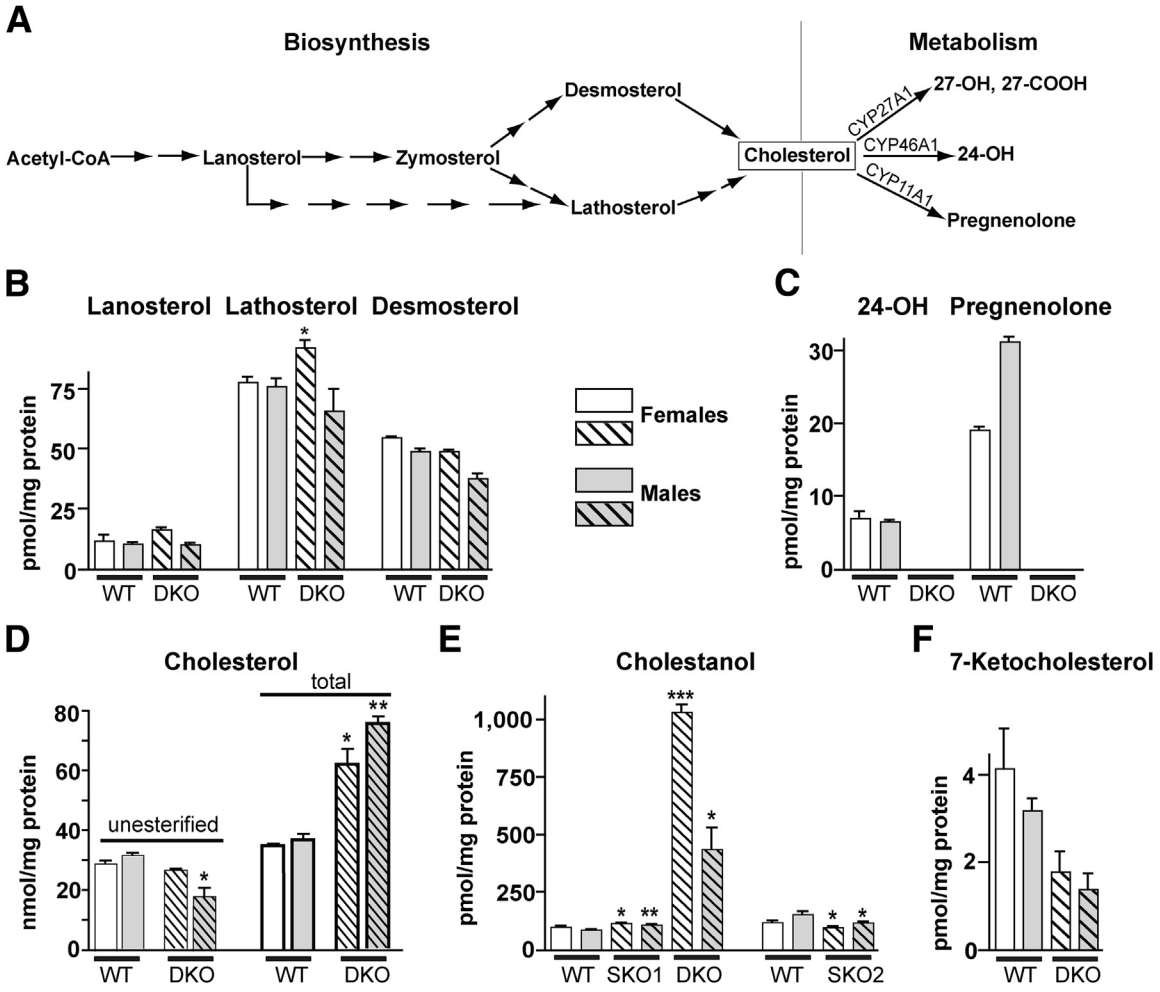

Figure 1 Altered sterol profile in the *Cyp27a1*$^{-/-}$*Cyp46a1*$^{-/-}$ retina. **A:** A simplified scheme of cholesterol biosynthesis and initial steps of metabolism showing the sterols quantified in **B**–**F**. Quantification of lanosterol, lathosterol, and desmosterol (**B**); 24-OH and pregnenolone (**C**); cholesterol (**D**); cholestanol, a product of the bile acid intermediate 7α-hydroxy-4-cholesten-3-one (**E**); and 7-ketocholesterol (**F**). The results are the means of triplicate measurements of the pooled retinal samples ($n = 40$ per sex per genotype); error bars indicate SEM and represent technical variability. Because *Cyp46a1*$^{-/-}$ and *Cyp27a1*$^{-/-}$*Cyp46a1*$^{-/-}$ mice were on a background (C57BL/6J;129S6/SvEv) different from that of *Cyp27a1*$^{-/-}$ mice (C57BL/6J), sterols in WT mice were measured in animals on two different background. Hatched bars indicate knockout mice while solid fill represents wild type. $^{*}P < 0.05$, $^{**}P < 0.01$, and $^{***}P < 0.001$. 7-Ketocholesterol, a product of cholesterol auto-oxidation; 24-OH, 24(S)-hydroxycholesterol; 27-COOH, 5-cholestenoic acid; 27-OH, 27-hydroxycholesterol; DKO, *Cyp27a1*$^{-/-}$*Cyp46a1*$^{-/-}$ mice; SKO1, *Cyp46a1*$^{-/-}$ mice; SKO2, *Cyp27a1*$^{-/-}$ mice; WT, *Cyp27a1*$^{+/+}$*Cyp46a1*$^{+/+}$ mice.

mechanisms of regulation of SOAT1, the major enzyme esterifying cholesterol.[43] Changes in the expression of *Cyp46a1*, *Akr1d1*, and *Cela3b* were confirmed by quantitative real-time PCR (qPCR). A 17.7-fold down-regulation of the nonfunctional *Cyp46a1* gene should not lead to metabolic consequences in *Cyp27a1*$^{-/-}$*Cyp46a1*$^{-/-}$ mice. A 3.6-fold up-regulation of *Akr1d1* is probably a part of a mechanism leading to increased retinal cholestanol levels because *Akr1d1* encodes Δ4-3-ketosteroid-5β-reductase, which metabolizes 7α-hydroxy-4-cholesten-3-one, a cholestanol precursor produced by the liver and known to flux in the brain across the blood-brain barrier in *Cyp27a1*$^{-/-}$ mice.[37,44] A similar mechanism could be operative in the retina of *Cyp27a1*$^{-/-}$*Cyp46a1*$^{-/-}$ mice. A 2.5-fold increase in retinal levels of *Cela3b*, encoding a serine protease elastase-3B and mainly expressed in the pancreas, was less understandable and investigated further. Normally, elastase-3B is secreted from the pancreas into the small intestine, where it becomes activated and participates in protein digestion.[45] During pancreatitis, however, elastase-3B is released in the blood, causing microvascular leakage and neutrophilic inflammation in distant organs.[46] To test for pancreatitis in *Cyp27a1*$^{-/-}$*Cyp46a1*$^{-/-}$ mice, we assessed pancreatic expression of *Cela3b* and two proinflammatory genes, *Tnfα* and *Il6*, as markers of inflammation. The pancreatic Cela3b levels were sevenfold higher in *Cyp27a1*$^{-/-}$*Cyp46a1*$^{-/-}$ than *Cyp27a1*$^{+/+}$*Cyp46a1*$^{+/+}$ mice, but the Tnfα and Il6 levels were decreased, 5- and 2.5-fold, respectively, indicating a lack of inflammation. An increased pancreatic expression of elastase-3B, which binds cholesterol and has been suggested to be involved in the intestinal transport of cholesterol,[47] could represent a body's compensatory response to a decreased cholesterol solubilization in the intestine due to a decreased production of bile acids as a result of CYP27A1 deficiency. Similarly, elastase-3B could be involved in transport of cholesterol in the retina and become up-regulated in *Cyp27a1*$^{-/-}$*Cyp46a1*$^{-/-}$ mice because of the accumulation of retinal cholesterol.

Pathological Features in the *Cyp27a1*$^{-/-}$*Cyp46a1*$^{-/-}$ Retina

In vivo examination of mice by SD-OCT revealed multiple bilateral hyperreflective spots that were localized throughout the *Cyp27a1*$^{-/-}$*Cyp46a1*$^{-/-}$ retina (Figure 3, A and D).

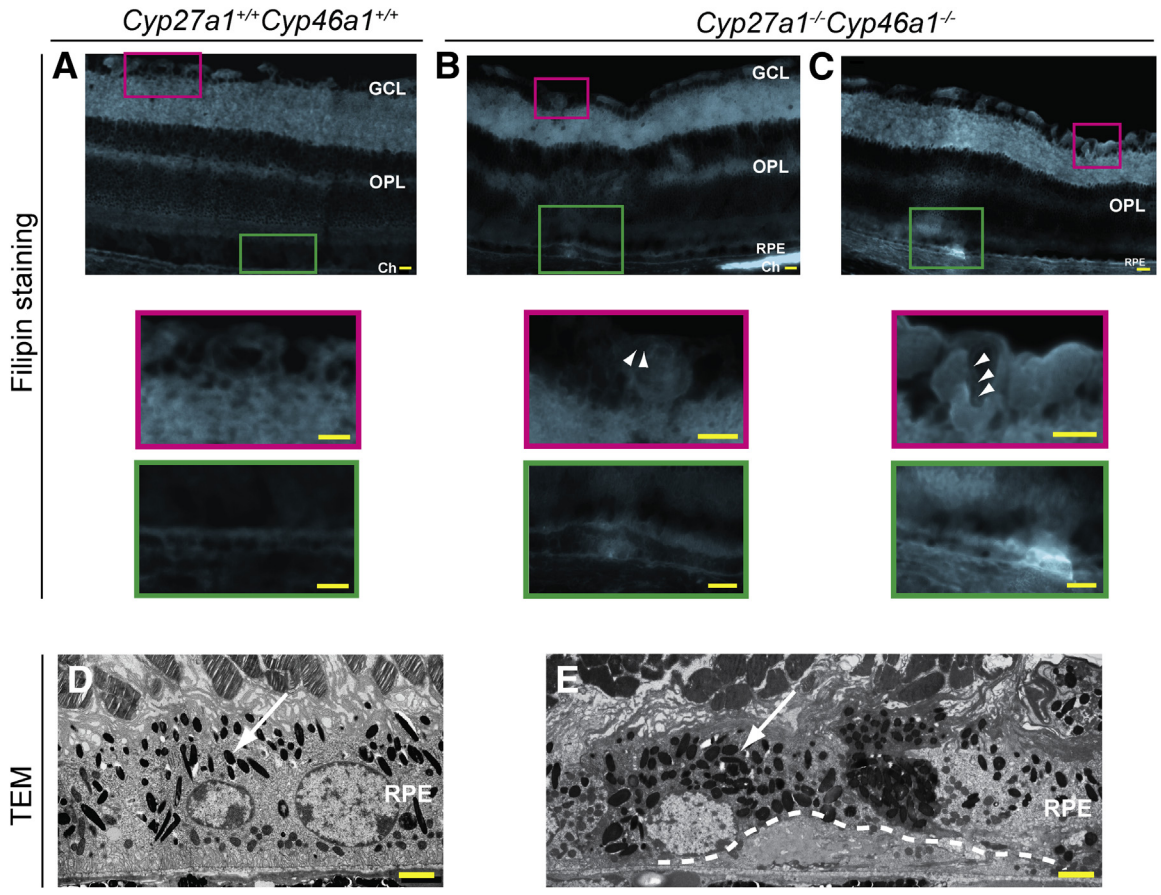

Figure 2 Sterol deposition in the retina and choroid of *Cyp27a1*$^{-/-}$*Cyp46a1*$^{-/-}$ mice. Detection of UC with filipin (in cyan) in a representative *Cyp27a1*$^{+/+}$*Cyp46a1*$^{+/+}$ retina (**A**) and different areas of a representative *Cyp27a1*$^{-/-}$*Cyp46a1*$^{-/-}$ retina (**B** and **C**). Colored boxes represent enlarged regions of **A**, **B**, and **C**. **White arrowheads** point to sterol deposits in the vascular wall. TEM of representative *Cyp27a1*$^{+/+}$*Cyp46a1*$^{+/+}$ (**D**) and *Cyp27a1*$^{-/-}$*Cyp46a1*$^{-/-}$ (**E**) mice. **White arrows** point to granules (either melanosomes or lipofuscin). **White dashed line** in **E** outlines the deposit. Scale bars: 100 μm (**A**–**C**); 2 μm (**D** and **E**). Ch, choroid; GCL, ganglion cell layer; OPL, outer plexiform layer; RPE, retinal pigment epithelium.

Males had more spots than females (90% versus 75% at 3 months of age) (Supplemental Figure S2A), consistent with a higher level of their total retinal cholesterol. When examined in cross section, the areas of increased light reflection represented hyperreflective whorl-like structures at the interface between the outer plexiform layer (OPL) and the outer nuclear layer (ONL) as well as disturbances in the PR ISs (Figure 3B). These abnormalities (confirmed by histological examination) (Supplemental Figure S2C) did not resolve with age, and instead often increased in size (Figure 3E). In some cases, they coalesced to form a patent RCA, as indicated by the Doppler flow of SD-OCT (Figure 3F). The *Cyp27a1*$^{+/+}$*Cyp46a1*$^{+/+}$ littermates also had hyperreflective spots on SD-OCT (Figure 3G). However, these spots were observed only at the OPL/ONL interface (Figure 3H and Supplemental Figure S2C), were less frequent and much smaller than in *Cyp27a1*$^{-/-}$*Cyp46a1*$^{-/-}$ mice (Supplemental Figure S2A and Figure 3H), and did not grow with age. These spots probably represented the manifestation of the naturally occurring mutation in the crumbs homolog 1 gene (*Crb1*^{rd8}), which is present in mouse strain C57BL/6N from common commercial vendors and which leads to specific retinal lesions when homozygous.[48,49] In our colony, 80% and 15% of *Cyp27a1*$^{-/-}$*Cyp46a1*$^{-/-}$ mice and their matching *Cyp27a1*$^{+/+}$ *Cyp46a1*$^{+/+}$ littermates were homozygous and heterozygous for *Crb1*^{rd8}, respectively, whereas 5% lacked this mutation. Despite the high prevalence of the *Crb1*^{rd8} allele in our colony, only modest *Crb1*^{rd8}-related lesions were observed compared with the reported manifestation of this allele in C57BL/6N mice.[48–50] This may reflect a background effect, because our animals were on a mixed C57BL/6J;129S6/SvEv background, and the C57BL/6J background is known to suppress the *Crb1*^{rd8} phenotype.[51,52] To control for possible contributions of the *Crb1*^{rd8} mutation to the pathological phenotype, we only made comparisons between *Cyp27a1*$^{-/-}$*Cyp46a1*$^{-/-}$ mice and their *Cyp27a1*$^{+/+}$*Cyp46a1*$^{+/+}$ littermates.

RCAs were not the only vascular pathological feature noted in the *Cyp27a1*$^{-/-}$*Cyp46a1*$^{-/-}$ retina. FA revealed additional vascular abnormalities, none of which were observed in *Cyp27a1*$^{+/+}$*Cyp46a1*$^{+/+}$ littermates. The most prominent lesion was the increased permeability of blood vessels, as indicated by imaging at early, intermediate, and late phases of FA. Vascular leakage was always observed around the RCAs (Figure 4, F–H), with a typical RCA pattern of fluorescein hyperfluorescence.[53] In some areas, however, the pattern of FA was different (Figure 4, O–Q) and did not seem to be associated with an RCA. FA also revealed areas of vascular nonperfusion (Figure 4, J–M), arteriovenous shunts (Figure 4, O–Q), localized vascular deformations (Figure 4R), and focal defects (Figure 4R).

Retinal characterizations by TEM and elastase digests provided additional findings. TEM documented a blood vessel

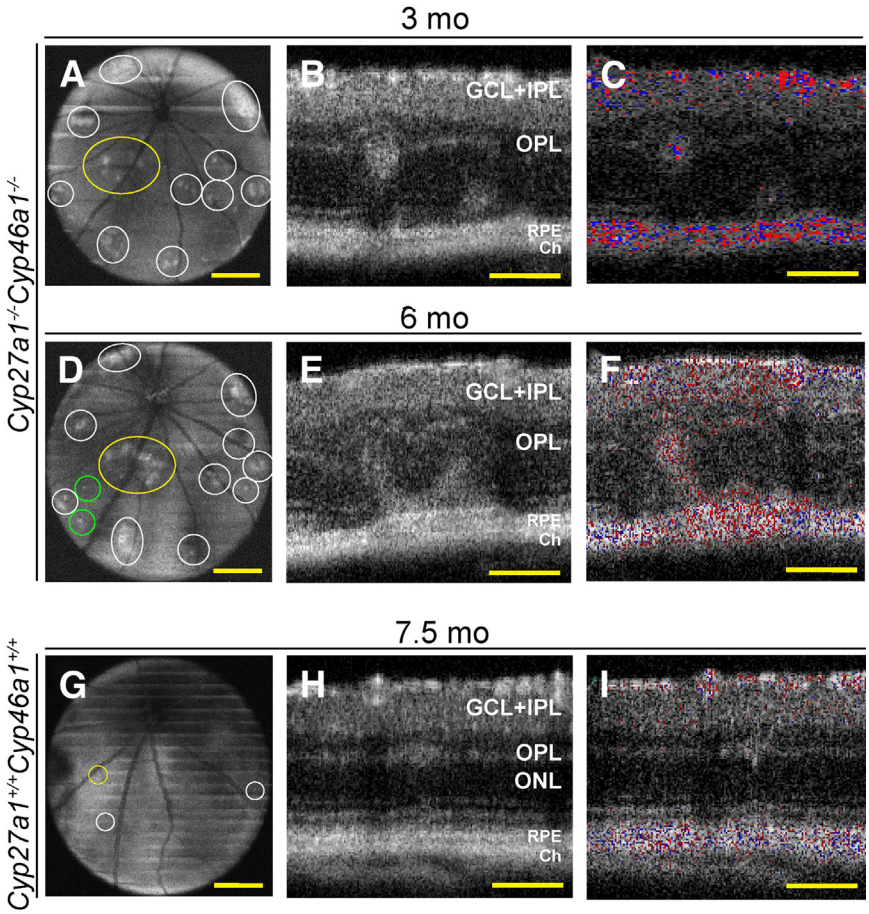

Figure 3 Retinal abnormalities in *Cyp27a1*$^{-/-}$ *Cyp46a1*$^{-/-}$ mice. Representative SD-OCT fundus depth images (50-degree field of view) at the OPL in the *Cyp27a1*$^{-/-}$*Cyp46a1*$^{-/-}$ animal (**A** and **D**) and sex-matched *Cyp27a1*$^{+/+}$*Cyp46a1*$^{+/+}$ littermate (**G**). Areas of pathology are outlined by **ovals** and **circles**. The areas examined in cross section (yellow) and the newly formed lesions (green). SD-OCT cross sections through the lesion area in the *Cyp27a1*$^{-/-}$*Cyp46a1*$^{-/-}$ retina (**B** and **E**) and the manifestation of the *Crb1*^{rd8} mutation in the *Cyp27a1*$^{+/+}$*Cyp46a1*$^{+/+}$ retina (**H**). Approximately 80% of *Cyp27a1*$^{-/-}$*Cyp46a1*$^{-/-}$ mice and matching *Cyp27a1*$^{+/+}$*Cyp46a1*$^{+/+}$ littermates are homozygous for *Crb1*^{rd8}, approximately 15% are heterozygous, and approximately 5% lack the mutation. The Doppler flow (**C**, **F**, and **I**) of **B**, **E**, and **H** showing the RCA (**F**) and the separation of the retinal and choroidal vascular networks (**C** and **I**). The pattern of SD-OCT changes is similar in males and females and between animals with a different number of hyperreflective spots. Scale bars: 300 μm (**A**, **D**, and **G**); 100 μm (**B**, **C**, **E**, **F**, **H**, and **I**). Ch, choroid; GCL, ganglion cell layer; IPL, inner plexiform layer; mo, months; ONL, outer nuclear layer; OPL, outer plexiform layer; RPE, retinal pigment epithelium; SD-OCT, spectral-domain optical coherence tomography.

protruding into the normally avascular RPE in the *Cyp27a1*$^{-/-}$*Cyp46a1*$^{-/-}$ retina and showed thickening of the basement membrane in this anastomosing blood vessel (Figure 4N). Basal membrane infoldings were lost in affected RPE cells, likely impairing their absorption and secretion. The elastase digests revealed retinal capillary degeneration, hypercellular blood vessels (dilated and nondilated), areas of condensed retinal vasculature, and areas containing membrane sheets (Figure 4, T and U). Thus, ablation of retinal cholesterol metabolism leads to pronounced effects on retinal vasculatures, with features shared with type 3 neovascular AMD (RCAs) and also diabetic retinopathy (vascular nonperfusion, capillary degeneration, increased vascular permeability, and thickening of the vascular basement membrane).[54–56]

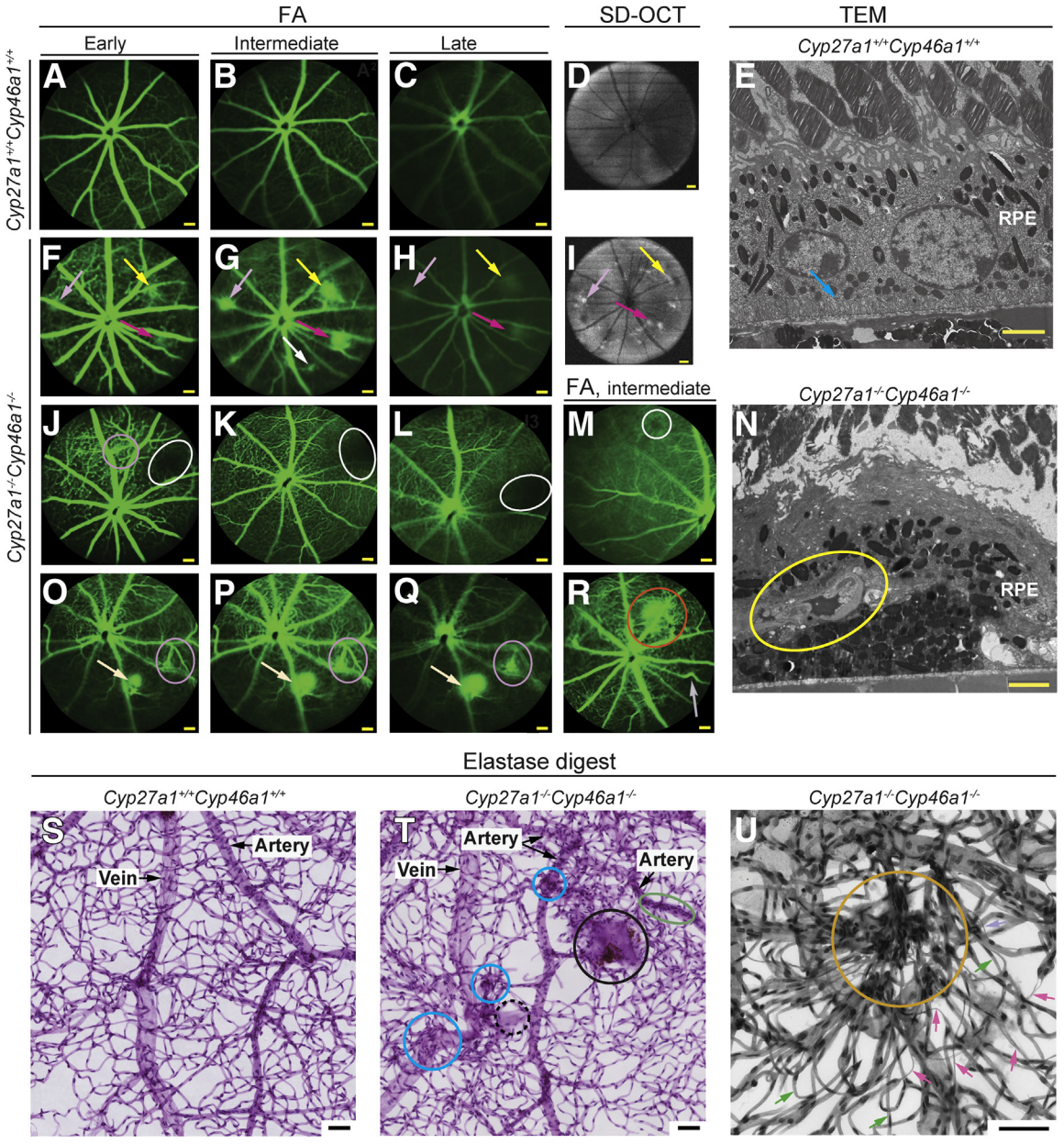

Figure 4 Different types of vascular abnormalities in the *Cyp27a1*$^{-/-}$*Cyp46a1*$^{-/-}$ retina. Fluorescein angiography (FA) of *Cyp27a1*$^{+/+}$*Cyp46a1*$^{+/+}$ (**A**–**C**) and the vascular leakage (**arrows** of the same color indicate the same lesion) of *Cyp27a1*$^{-/-}$*Cyp46a1*$^{-/-}$ mice (**F**–**H**, **J**–**M**, and **O**–**R**). SD-OCT fundus images (50-degree field of view) (**D** and **I**). TEM of the retinal cross section through the representative lesion (**yellow arrow** in **F**–**I**) with vascular leakage documenting a blood vessel in the RPE (**yellow oval**) and no membrane infoldings (**blue arrow** in **E**) (**N**). Representative FA images of other types of vascular abnormalities in *Cyp27a1*$^{-/-}$*Cyp46a1*$^{-/-}$ mice (**J**–**M** and **O**–**R**); vascular nonperfusion (**white ovals** and **circle**) (**J**–**M**); arteriovenous shunts (**fuchsia ovals**) (**J** and **O**–**Q**); and vascular deformations (**gray arrow**) and focal defects (red circle) (**R**). Retinal analyses by elastase digests (**S**–**U**) show nondilated and dilated hypercellular blood vessels (**green oval** and **blue circles**, respectively, in **T**); membrane sheets with and without pigment (**solid** and **dashed black circles**, respectively, in **T**); intraretinal microvascular abnormality consisting of hypercellular condensed retinal vasculature (**orange circle** in **U**); and degenerated capillaries (**magenta arrows** in **U**; **green arrows** point to normal capillaries). Scale bars: 100 μm (**A**–**C**, **F**–**H**, **J**–**M**, and **O**–**R**); 2 μm (**E** and **N**); 50 μm (**S**–**U**). RPE, retinal pigment epithelium; SD-OCT, spectral-domain optical coherence tomography.

To test whether increased permeability of retinal blood vessels is associated with a leakage of lipids, retinal cross sections were stained with oil red O, an oil-soluble dye that labels tissue deposits of fat. The *Cyp27a1*$^{-/-}$*Cyp46a1*$^{-/-}$ retinas had localized areas of intense ruby color (Figure 5A), whereas the *Cyp27a1*$^{+/+}$*Cyp46a1*$^{+/+}$ retinal layers had faint and uniform oil red O staining (Figure 5K). The oil red O–stained spots in the *Cyp27a1*$^{-/-}$*Cyp46a1*$^{-/-}$ retinas varied in size and location and were present in the normally vascular GCL and INL as well as in the normally avascular ONL and PR. These sections were then restained with tomato lectin, which labels blood vessels, microglia, and sometimes PRs.[57,58] The lectin signals were larger and more intense in the *Cyp27a1*$^{-/-}$*Cyp46a1*$^{-/-}$ than in the *Cyp27a1*$^{+/+}$*Cyp46a1*$^{+/+}$ retinas (Figure 5, B, G, and L), suggesting blood vessel dilation and microglia activation. In some cases, the lectin staining colocalized with the areas of intense oil red O staining (Figure 5, C and H). TEM imaging confirmed lipid leakage from the *Cyp27a1*$^{-/-}$*Cyp46a1*$^{-/-}$ retinal vasculature by demonstrating lipid deposition inside and adjacent to blood vessels (Figure 5D). In contrast, no lipid accumulations were noted in the blood vessels of the systemic circulation, as indicated by the oil red O staining of the aortic root of the heart (Figure 5J), a preferred site for the atherosclerotic lesion formation in mice.[33] In the *Cyp27a1*$^{-/-}$*Cyp46a1*$^{-/-}$ retina, lipid droplets were also noted in the intraretinal space away from blood vessels (Figure 5E) and in the RPE (Figure 5I), where they contained multilamellar circular structures resembling myelin figures, which are typically connected to a reservoir of dense lipid plaques.[59] The presence of lipid droplets at locations away from blood vessels suggests that their accumulation is the result of the dysfunctional cholesterol metabolism rather than increased permeability of blood vessels. Thus, lipid accumulation in the *Cyp27a1*$^{-/-}$*Cyp46a1*$^{-/-}$ retina seems to occur via two processes, vascular abnormalities and metabolic changes.

To examine overall retinal function, ERGs were recorded under dark- and light-adapted conditions from 3- and 6-month-old mice (Supplemental Figure S3). Dark-adapted (scotopic) ERGs of 3-month-old *Cyp27a1*$^{-/-}$*Cyp46a1*$^{-/-}$ female and male mice were not significantly different from those of *Cyp27a1*$^{+/+}$*Cyp46a1*$^{+/+}$ controls. Light-adapted (photopic) ERGs were also comparable at this age. When examined at 6 months of age, dark-adapted ERGs of *Cyp27a1*$^{-/-}$*Cyp46a1*$^{-/-}$ mice were reduced lower than those of controls for both females and males. The amplitude reductions were statistically significant for males, consistent with the higher frequency of lesions in the males in comparison to the females. This sex-specific difference was also seen in light-adapted (photopic) ERGs, where in comparison to controls, cone ERGs of only males were significantly reduced in amplitude.

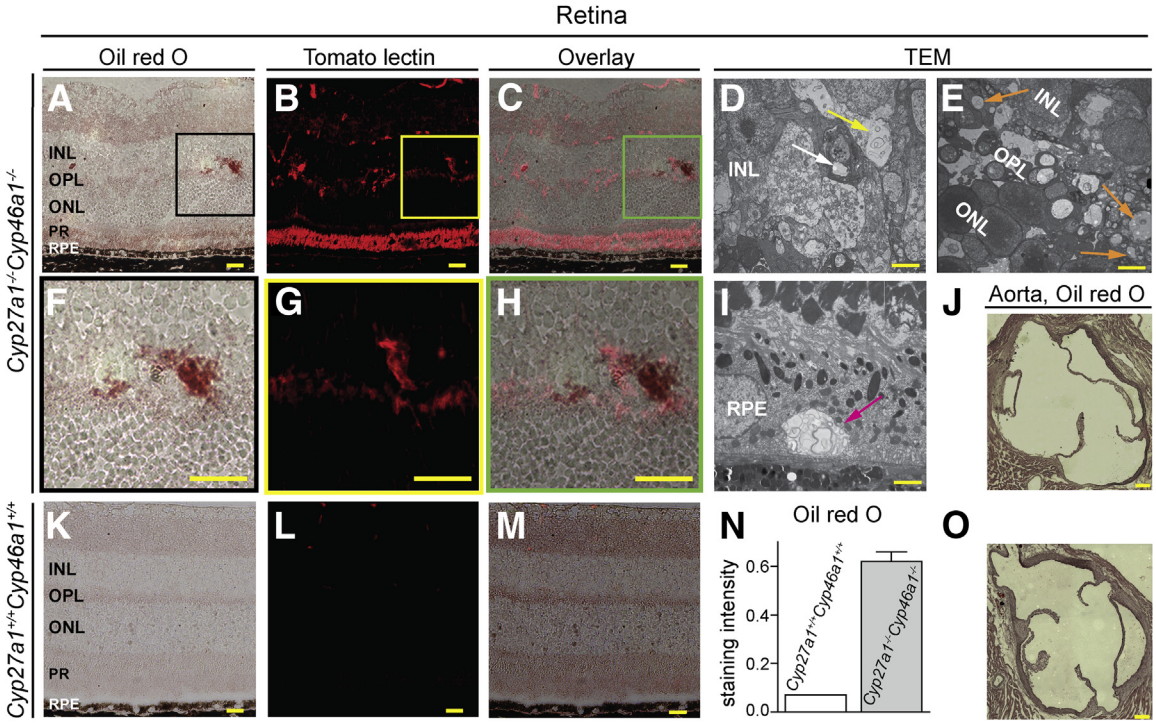

Figure 5 Focal lipid accumulation in the *Cyp27a1*$^{-/-}$*Cyp46a1*$^{-/-}$ retina. Representative staining of the cross section through the area of pathology in the *Cyp27a1*$^{-/-}$*Cyp46a1*$^{-/-}$ retina (**A**–**C**) and the corresponding region in the *Cyp27a*$^{+/+}$*Cyp46a1*$^{+/+}$ retina (**K**–**M**). **N:** Histological quantifications. Representative staining of the cross sections through the aortic root of the heart in the *Cyp27a1*$^{-/-}$*Cyp46a1*$^{-/-}$ (**J**) and *Cyp27a1*$^{+/+}$*Cyp46a1*$^{+/+}$ (**O**) mice. Enlarged view of the boxed regions in **A**–**C** (**F**–**H**). TEM of the *Cyp27a1*$^{-/-}$*Cyp46a1*$^{-/-}$ retina confirm lipid deposition inside and outside blood vessels (**white** and **yellow arrows**, respectively, in **D**), away from blood vessels (**orange arrows**, **E**), and in the RPE (**magenta arrow**, **I**). Scale bars: 100 μm (**A**–**C**, **F**–**H**, **J**, **K**–**M**, and **O**); 2 μm (**D** and **E**); 1 μm (**I**). INL, inner nuclear layer; ONL, outer nuclear layer; OPL, outer plexiform layer; PR, photoreceptor; RPE, retinal pigment epithelium.

Nonocular Manifestations of *Cyp27a1*$^{-/-}$*Cyp46a1*$^{-/-}$ Deficiency

The retinal abnormalities in *Cyp27a1*$^{-/-}$*Cyp46a1*$^{-/-}$ mice prompted us to evaluate nonocular organs to determine whether these changes reflect a system phenotype. Visual inspection of *Cyp27a1*$^{-/-}$*Cyp46a1*$^{-/-}$ animals revealed that they were lean and had an altered appearance of three nonocular systems: lungs, liver, and spleen (Figure 6 and Supplemental Figure S4). The lungs had a milky appearance in both *Cyp27a1*$^{-/-}$*Cyp46a1*$^{-/-}$ males and females, likely due to focal accumulation of neutral lipids mainly present in perivascular regions (Figure 6B). The color of the *Cyp27a1*$^{-/-}$*Cyp46a1*$^{-/-}$ liver was also milky in both sexes (Supplemental Figure S4B), consistent with a significant increase in the amount of neutral lipids and esterified cholesterol (Figure 6, E–G). Lipid

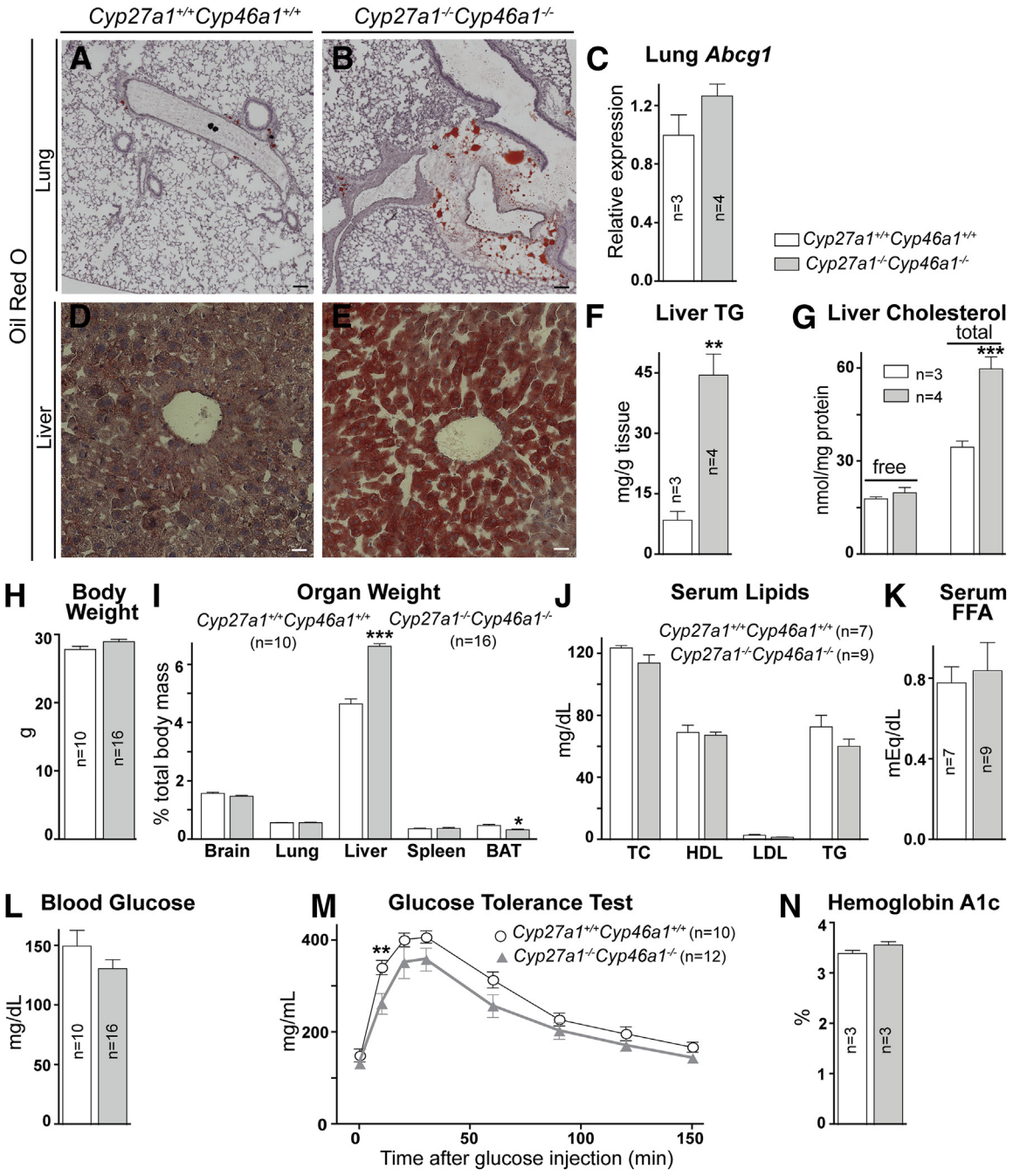

Figure 6 Nonocular manifestations of *Cyp27a1*$^{-/-}$*Cyp46a1*$^{-/-}$ deficiency. Increased content of neutral lipids in the lungs (**A** and **B**) and livers (**D** and **E**), as indicated by histochemistry and quantitative measurements (**F** and **G**). **I:** The liver weight is increased in *Cyp27a1*$^{-/-}$*Cyp46a1*$^{-/-}$ mice, whereas the amount of brown adipose tissue (BAT) is decreased. The lung Abcg1 levels (**C**), total body weight (**H**), serum lipids (TC, total cholesterol) (**J**), serum free fatty acids (FFAs; **K**), fasting blood glucose (**L**), and hemoglobin A_{1c} (**N**) are unchanged in *Cyp27a1*$^{-/-}$*Cyp46a1*$^{-/-}$ mice; however, tolerance to glucose (**M**) is improved. $^{**}P < 0.01$, $^{***}P < 0.001$. Scale bar = 100 μm (**A**, **B**, **D**, and **E**).

accumulation could contribute to the liver enlargement noted in *Cyp27a1*$^{-/-}$*Cyp46a1*$^{-/-}$ mice. There was a trend toward increased spleen weight in *Cyp27a1*$^{-/-}$*Cyp46a1*$^{-/-}$ males (Figure 6I), and a statistically significant increase in the organ weight in *Cyp27a1*$^{-/-}$*Cyp46a1*$^{-/-}$ females older than 13 months (Supplemental Figure S4D). The amount of total body fat was reduced in both *Cyp27a1*$^{-/-}$*Cyp46a1*$^{-/-}$ sexes, as indicated by the measurements of the interscapular brown fat, yet the body weight was unchanged compared with the *Cyp27a1*$^{+/+}$*Cyp46a1*$^{+/+}$ mice (Figure 6, H and I, and Supplemental Figure S4C). Despite changes in the lungs, liver, and amount of fat, the levels of serum lipids, free fatty acids, glucose, and hemoglobin A_{1c} (an indicator of a long-term blood sugar control) were essentially unchanged in *Cyp27a1*$^{-/-}$*Cyp46a1*$^{-/-}$ mice of both sexes compared with *Cyp27a1*$^{+/+}$*Cyp46a1*$^{+/+}$ animals (Figure 6, L and N); *Cyp27a1*$^{-/-}$*Cyp46a1*$^{-/-}$ mice even showed an improved tolerance to glucose (Figure 6M). Overall, serum analyses demonstrated that the abnormalities noted in the *Cyp27a1*$^{-/-}$*Cyp46a1*$^{-/-}$ retina were unlikely due to an altered chemistry in the systemic circulation. Hence, we focused on the retina again and investigated some of the processes that could be triggered by cholesterol accumulation and impaired production of oxysterols.

Immune Response of the *Cyp27a1*$^{-/-}$*Cyp46a1*$^{-/-}$ Retina

The formation of abnormal anastomosing blood vessels motivated retinal evaluations by the angiogenesis PCR array, which profiles a diverse set of genes associated with pathological neovascularization (Supplemental Table S2 and Supplemental Figure S1). Of the 84 genes evaluated, the expression levels of only four were up-regulated by twofold in the *Cyp27a1*$^{-/-}$*Cyp46a1*$^{-/-}$ retinas in comparison to the *Cyp27a1*$^{+/+}$*Cyp46a1*$^{+/+}$ retinas. These included the genes encoding proinflammatory cytokine *Tnfα*, chemokines *Ccl2* and *Cxcl2*, and the receptor for the fibroblast growth hormone (*Fgfr3*). RT-qPCR validated the PCR array data and demonstrated that the increases in the gene expression are moderate (up to 6.5-fold) in the *Cyp27a1*$^{-/-}$*Cyp46a1*$^{-/-}$ retinas, suggesting that either the up-regulation of proinflammatory genes occurs only in specific retinal cells or that the inflammation is of a low grade.

Macrophages constitute a cell type where proinflammatory genes could be up-regulated by deficiency of CYP27A1 and CYP46A1, because oxysterols activate LXRs in macrophages, and synthetic LXR agonists suppress a set of inflammatory genes in these cell types.[60] To pursue this idea, retinal flat mounts were treated with antibodies against F4/80, and retinal cross sections were stained for Iba1, two different markers for macrophageal/microglial activation.[61] At the level of the inner retina, the *Cyp27a1*$^{-/-}$*Cyp46a1*$^{-/-}$ flat mounts showed F4/80-positive cells, which had stout cell bodies and thick cell processes (Figure 7, A and B), indicative of macrophage activation. There was also faint anti-F4/80 staining at the level of the outer retina (Figure 7, C and D). Anti-F4/80 staining was not detected in either the inner or outer retina of *Cyp27a1*$^{+/+}$

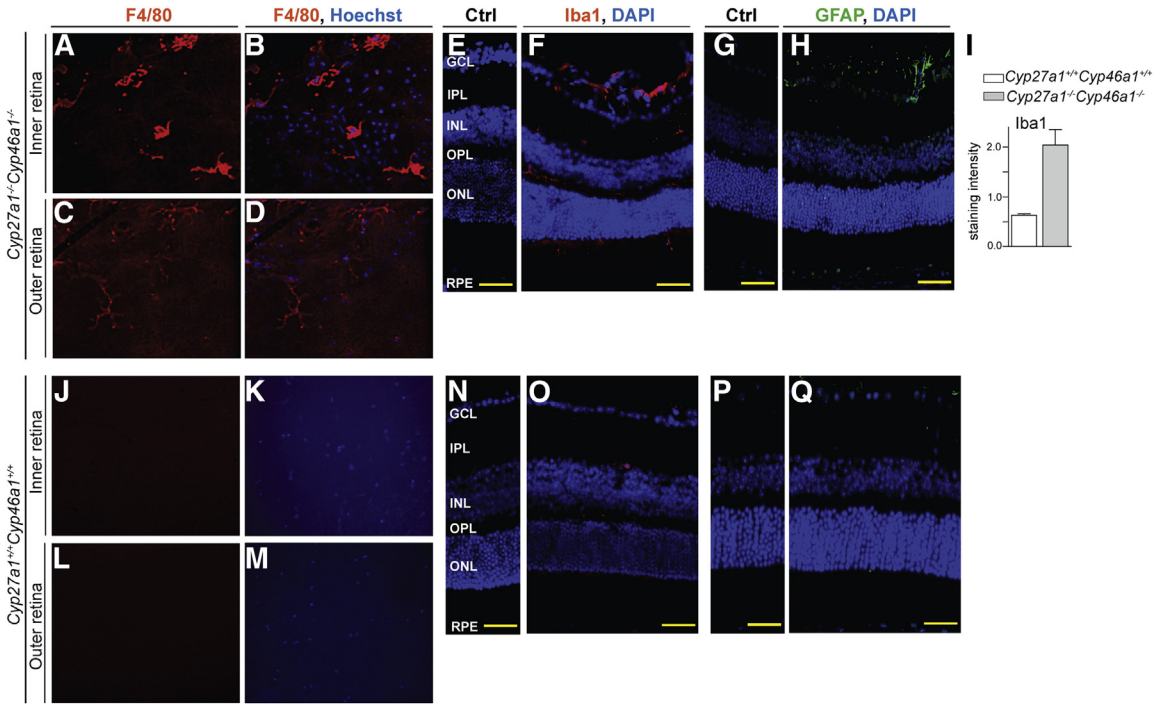

Figure 7 Macrophages/microglia activation in the *Cyp27a1*$^{-/-}$*Cyp46a1*$^{-/-}$ retina. Representative staining of the retinal flat mounts for F4/80 (**A**–**D**) and retinal cross sections for Iba1 (**E** and **F**) and GFAP (**G** and **H**). Corresponding images for a *Cyp27a1*$^{+/+}$*Cyp46a1*$^{+/+}$ mouse (**J**–**Q**). **I:** Histological quantifications. Nuclei were stained with Hoechst (**B**, **D**, **K**, and **M**) or DAPI (**E**–**H** and **N**–**Q**). Control sections (Ctrl) were treated with the serum from nonimmunized animals. Scale bar = 100 μm (**E**–**H** and **N**–**Q**). GCL, ganglion cell layer; INL, inner nuclear layer; IPL, inner plexiform layer; ONL, outer nuclear layer; OPL, outer plexiform layer; RPE, retinal pigment epithelium.

Cyp46a1$^{+/+}$mice (Figure 7, J–M). Anti-Iba1 signal in retinal cross sections confirmed an increased number of macrophage/microglial cells in the *Cyp27a1*$^{-/-}$*Cyp46a1*$^{-/-}$ inner retina and revealed microglia/macrophage migration to the subretinal space (Figure 7F). Iba1 labeling in the ONL and subretinal space is not usually observed in pigmented mice[61] and was not noted in *Cyp27a1*$^{+/+}$*Cyp46a1*$^{+/+}$ littermates (Figure 7O).

This evidence of activated macrophage/microglial cells led us to stain for CD11b, the α_M subunit of the $\alpha_M\beta_2$ integrin, an adhesion receptor expressed on the surface of monocytes (precursors of macrophages in the blood) and other leukocytes.[62] Anti-CD11b signal was elevated inside retinal blood vessels of *Cyp27a1*$^{-/-}$*Cyp46a1*$^{-/-}$ mice (Figure 8, B and U), suggesting the activation of the receptor-containing cells or more leukocytes in blood. When activated, the $\alpha_M\beta_2$-containing blood cells usually adhere to the vascular endothelium, which triggers various events, including inflammation and increased production of reactive oxygen species.[62,63] Hence, we next stained for C3 and C3a. C3 is central to all complement activation pathways, and C3a is an anaphylatoxin and mediator of local inflammatory responses.[64] Increased expression of C3 in mouse retina has been shown to lead to significantly increased vascular permeability.[65] Consistent with the abnormal blood vessel leakage in the *Cyp27a1*$^{-/-}$*Cyp46a1*$^{-/-}$ retina, an anti-C3/C3a signal was detected and was mostly associated with blood vessels (Figure 8D). We next stained the retina for complement factor C9, an indicator of the assembly of the terminal membrane attack complex, which disrupts the

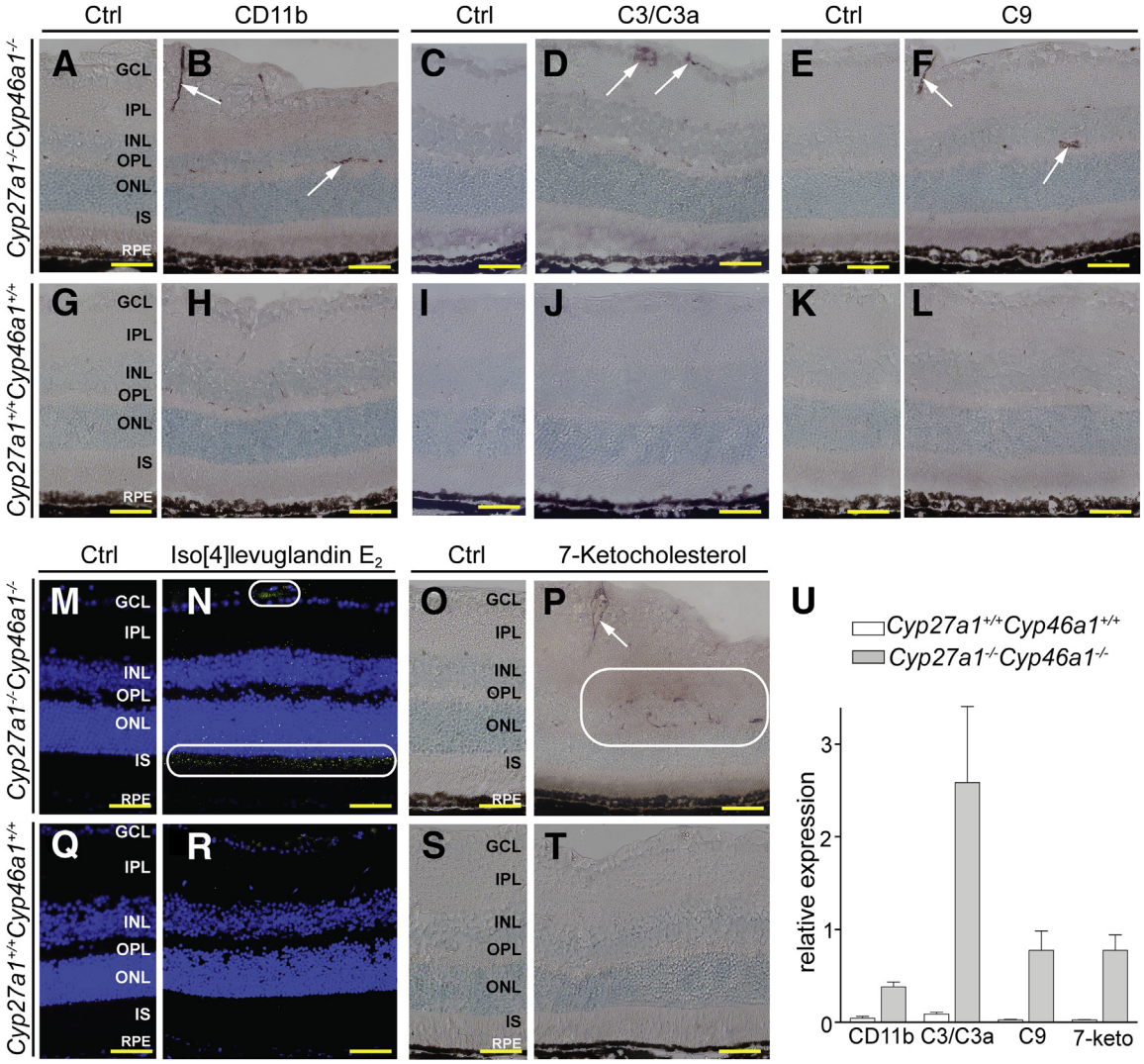

Figure 8 Increased inflammatory response and oxidative stress in the *Cyp27a1*$^{-/-}$*Cyp46a1*$^{-/-}$ retina. Representative stainings for the $\alpha_M\beta_2$ integrin (CD11b) (**A** and **B**), complement factors C3/C3a and C9 (**C**–**F**), iso[4]levuglandin E_2 (**M** and **N**), and 7-ketocholesterol (7-keto; **O** and **P**). Corresponding images for a *Cyp27a1*$^{+/+}$*Cyp46a1*$^{+/+}$ mouse (**G**–**L** and **Q**–**T**). Control sections (Ctrl) were treated with the serum from nonimmunized animals. **White arrows** and **rounded rectangles** indicate increased staining compared with the *Cyp27a1*$^{+/+}$*Cyp46a1*$^{+/+}$ retinas. Immunostaining for 7-ketocholesterol likely represents antibody binding to both esterified and unesterified forms of the sterol, whereas the measurements in Figure 1 are of unesterified 7-ketocholesterol only. **U:** Histological quantifications. Scale bar = 100 μm (**A**–**T**). GCL, ganglion cell layer; INL, inner nuclear layer; IPL, inner plexiform layer; IS, inner segment; ONL, outer nuclear layer; OPL, outer plexiform layer; RPE, retinal pigment epithelium.

target cell membranes and leads to cell lysis.[66] C9 staining was also increased in the *Cyp27a1*$^{-/-}$*Cyp46a1*$^{-/-}$ retina, where it was mainly restricted to blood vessels (Figure 8F).

Müller cells, the predominant glial cells of the retina, contribute to the blood-retinal barrier. Hence, pathological processes in retinal vasculature in *Cyp27a1*$^{-/-}$*Cyp46a1*$^{-/-}$ mice could lead to activation of Müller cells or vice versa. The retina was stained for glial fibrillary acidic protein (GFAP), an intermediate filament protein up-regulated in Müller cells in response to different insults.[67] Anti-GFAP immunoreactivity was detected everywhere in *Cyp27a1*$^{-/-}$*Cyp46a1*$^{-/-}$, but not *Cyp27a1*$^{+/+}$*Cyp46a1*$^{+/+}$, retinas (Figure 7, H and Q) and was primarily localized to the GCL, the major site for the GFAP immunoreactivity in Müller cells,[68] which span the entire thickness of the retina. Faint, punctate staining was also present in the INL containing Müller somas, the normally avascular ONL, and also in the RPE, resembling a staining pattern reported in patients with AMD.[69] In the areas of vascular abnormalities, GFAP staining was more pronounced and encompassed longer regions of the Müller cells.

Oxidative stress is a common factor that could lead to the activation of macrophages and Müller cells.[67,70] The presence of this pathological process in the *Cyp27a1*$^{-/-}$*Cyp46a1*$^{-/-}$ retina was assessed by staining for two lipids: isolevuglandins (isoLGs) and 7-ketocholesterol, oxidation products of arachidonate and cholesterol, respectively.[71,72] Adducts of isoLGs with proteins and phospholipids serve as long-term biomarkers of oxidative stress, and are found at increased concentrations in plasma and vasculature of patients with atherosclerosis and in plasma of patients with AMD.[73,74] 7-Ketocholesterol is a proinflammatory and pro-apoptotic oxysterol produced nonenzymatically from cholesterol and shown to induce inflammation and angiogenesis *in vivo*.[75] The isoLG signal was detected inside the blood vessels of the GCL in both the *Cyp27a1*$^{-/-}$*Cyp46a1*$^{-/-}$ and *Cyp27a1*$^{+/+}$ *Cyp46a1*$^{+/+}$ retinas, but was much higher in the *Cyp27a1*$^{-/-}$ *Cyp46a1*$^{-/-}$ retina (Figure 8, M, N, Q, and R). This staining, along with that for CD11b, is in agreement with previous studies showing that isoLGs can modify plasma LDL and be recognized by macrophages.[76,77] The *Cyp27a1*$^{-/-}$*Cyp46a1*$^{-/-}$ retina also had a much stronger isoLG signal in the ISs, where light-induced oxidative stress leads to the formation of isoLGs and alterations of mitochondrial morphological features.[31] The pattern of staining for 7-ketocholesterol was different, because the signal was only associated with the wall of retinal blood vessels and was present only in *Cyp27a1*$^{-/-}$*Cyp46a1*$^{-/-}$ mice (Figure 8, O, P, S, and T). IsoLG and 7-ketocholesterol staining documented elevated oxidative stress in specific regions of the *Cyp27a1*$^{-/-}$*Cyp46a1*$^{-/-}$ retina.

Discussion

Our major findings are that global ablation of *Cyp27a1*$^{-/-}$ and *Cyp46a1*$^{-/-}$ in mice leads to retinal microangiopathy (Figure 4) and changes in several nonocular organs (Figure 6), but does not affect systemic lipid and glucose levels (Figure 6). Pathological processes identified in retinal blood vessels of *Cyp27a1*$^{-/-}$*Cyp46a1*$^{-/-}$ mice fit remarkably well the scenario of atherosclerosis,[70] although the retina contains only small arterioles instead of arteries. Therefore, in suggesting the putative sequence of early events ultimately leading to vascular lesions in the *Cyp27a1*$^{-/-}$*Cyp46a1*$^{-/-}$ retina (Figure 9), we used the current knowledge of atherosclerosis.

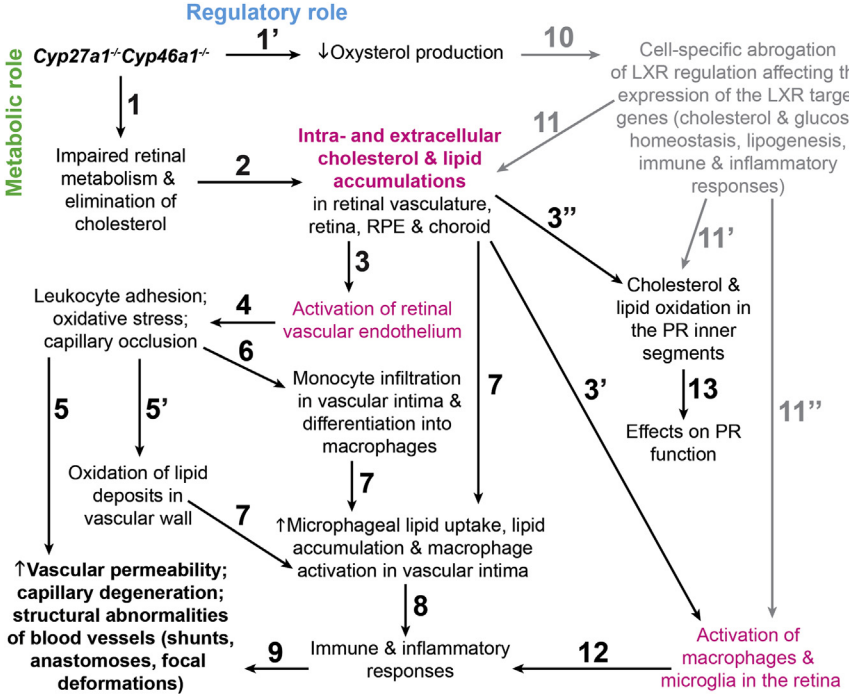

Figure 9 Proposed pathological events in the *Cyp27a1*$^{-/-}$*Cyp46a1*$^{-/-}$ retina. The sequence of events is numbered chronologically with primes (′,″), indicating events that may occur simultaneously, because CYP27A1 and CYP46A1 may have dual roles [eg, metabolic (green) and regulatory (blue) roles], and one event may trigger several parallel events. Events in magenta are suggested to play key roles in the proposed sequence. Gray indicates events that have not been confirmed experimentally (ie, event 10, abrogation of LXR regulation). All paths ultimately lead to the development of vascular abnormalities (boldfaced).

Atherosclerosis is thought to begin with the activation of vascular endothelium at sites with disturbed blood flow and subendothelial accumulations of lipids, usually as a result of the elevated plasma LDL levels.[70] *Cyp27a1*$^{-/-}$*Cyp46a1*$^{-/-}$ mice have a normolipidemic plasma profile (Figure 6), but their retinal vascular wall has sterol accumulations (Figure 2) and vascular endothelium is probably activated (Events 1 to 3, Figure 9), like in the systemic circulation of CYP27A1-deficient humans, who have premature atherosclerosis despite generally normal plasma cholesterol.[78,79] The atherosclerotic plaques in CYP27A1-deficient individuals contain more cholesterol than cholestanol (97.2% versus 2.8% of total sterol content), suggesting that cholesterol, rather than cholestanol, probably accumulates in retinal blood vessels and the choroidal network of *Cyp27a1*$^{-/-}$ *Cyp46a1*$^{-/-}$ mice.

When vascular endothelial cells are activated, they secrete chemokines that interact with receptors on monocytes, leading to monocyte recruitment.[80] In the *Cyp27a1*$^{-/-}$ *Cyp46a1*$^{-/-}$ retina, leukocyte adhesion to blood vessels (Event 4, Figure 9) is indicated by anti-CD11b staining (Figure 8) and could play a role in vascular leakage and capillary degeneration (Event 5, Figure 9). This will be similar to adherent leukocytes in diabetic retinopathy, which release cytokines and reactive oxygen species that damage retinal microvasculature and physically occlude capillaries.[55] Leukocyte accumulation when cholesterol load in vascular wall is increased also explains why cholesterol and other lipids are oxidized inside retinal blood vessels (Event 5′, Figure 9) and 7-ketocholesterol and isoLGs are detected (Figure 8).

In atherosclerosis, monocyte adhesion is followed by their infiltration into the subendothelial space and differentiation into macrophages, which begin to uptake nonoxidized and oxidized cholesterol-rich lipoprotein particles. This uptake stimulates the production of a variety of molecules, including inflammatory mediators, growth factors, and reactive oxygen species, leading to unresolved inflammation and the formation of a complex lesion.[70] Several of these atherosclerotic processes probably occur in the *Cyp27a1*$^{-/-}$*Cyp46a1*$^{-/-}$ retinal vasculature. Monocyte infiltration (Event 6, Figure 9), for example, is indicated by increased expression of *Ccl2* (Supplemental Figure S1), monocyte chemoattractant protein 1, which is one of the key chemokines that regulate the migration and infiltration of monocytes from the blood stream across the vascular endothelium.[81] An increase in macrophageal lipid uptake and macrophageal lipid concentrations (Event 7, Figure 9) could be due to cholesterol accumulation in the vascular wall (Event 2, Figure 9) and a lack of CYP27A1 in macrophages metabolizing uptaken cholesterol. In addition, a decreased production of oxysterols (Event 1′, Figure 9) could impair cholesterol removal via the LXR-controlled efflux (Events 10 and 11, Figure 9). Collectively, increased levels of cholesterol and the presence of 7-ketocholesterol (Events 2 and 5′, respectively, Figure 9), probably contribute to the macrophage activation (Event 7, Figure 9) as indicated by F4/80 and Iba1 staining (Figure 7). In the *Cyp27a1*$^{-/-}$*Cyp46a1*$^{-/-}$ retina, macrophage activation (Events 3′ and 11″, Figure 9) could be due to intracellular cholesterol accumulation and aberrant immune response, respectively, because the LXR suppression of inflammatory genes in macrophages could be impaired. Lymphocytes from mice lacking LXRβ were found to exhibit enhanced responses to homeostatic and antigen-driven challenges,[82] and the CYP46A1 metabolite, 24-hydroxycholesterol, was shown to suppress the activation of macrophageal inducible nitric oxide synthase.[83] The lack of the CYP27A1 metabolite, 27-hydroxycholesterol, is important in the *Cyp27a1*$^{-/-}$*Cyp46a1*$^{-/-}$ retina as well because vascular abnormalities in these mice do not fully overlap with those in *Cyp27a1*$^{-/-}$[12] or *Cyp46a1*$^{-/-}$ mice (under investigation). Impaired LXR signaling in *Cyp27a1*$^{-/-}$ *Cyp46a1*$^{-/-}$ mice is also implicated by some of their nonocular abnormalities that mirror those reported in *Lxrα*$^{-/-}$*β*$^{-/-}$ and *Abcg1*$^{-/-}$ (an LXR target) mice (Supplemental Table S3), although genotype-specific manifestations are observed.

Macrophage activation in the *Cyp27a1*$^{-/-}$*Cyp46a1*$^{-/-}$ retina probably leads to inflammatory processes in both the retina and retinal vasculature (Events 12 and 8, respectively, Figure 9) and the development of vascular abnormalities (Event 9, Figure 9). The inflammation in the retina is indicated by the up-regulation of retinal expression of *Cxcl2*, a cytokine encoding macrophage inflammatory protein 2α,[84] and of *Tnfα*, a proinflammatory cytokine produced chiefly by the activated macrophages (Supplemental Figure S1).[85] The inflammation inside the blood vessels is suggested by the activation of the complement pathway, documented through staining for complement factors C3/C3a and C9 (Figure 8). Complement factor C3 is important in the pathogenesis of AMD, whereas the terminal membrane attack complex, including C9, is deposited in retinal vessels of diabetic humans and is suggested to play a role in increased vascular permeability, leukostasis, and apoptosis of retinal capillary cells.[86,87] Our anti-C3/C3a and anti-C9 vascular localizations are consistent with pathological processes observed in retinal vasculature in AMD and diabetes and explain, in part, vascular abnormalities in the *Cyp27a1*$^{-/-}$ *Cyp46a1*$^{-/-}$ retina. The present work, linking the activation of retinal macrophages and retinal vascular abnormalities, is consistent with a previous investigation demonstrating that impaired cholesterol efflux in senescent macrophages promotes AMD.[88] Both studies, thus, emphasize the importance of the mechanisms that eliminate cholesterol in macrophages either via the lipoprotein pathway[88] or by cholesterol-specific enzymes (the present work). Our work also supports the previously suggested use of LXR agonists for the prevention of neovascular AMD[88] and diabetic retinopathy.[89] Pharmaceutical agents that increase the activity of CYP46A1 could be another option because they were shown to stimulate the production of 24-hydroxycholesterol in mouse brain[90] and, thus, have a potential to exert a similar effect in the retina.

PRs were recently identified as the major contributors to diabetes-induced oxidative stress in the retina and play an important role in the pathogenesis of diabetic retinopathy.[91] Similarly, there is an increased production of reactive

oxygen species in the ISs of the *Cyp27a1*$^{-/-}$*Cyp46a1*$^{-/-}$ retina (Events 3″ and 11′, Figure 9), as indicated by anti-isoLG staining (Figure 8). An increase in the oxidation of polyunsaturated fatty acids in the ISs could affect PR function[31] and explain a reduction in ERG amplitudes in *Cyp27a1*$^{-/-}$*Cyp46a1*$^{-/-}$ mice (Supplemental Figure S3 and Event 13, Figure 9). Additional studies are required to establish the contribution of the oxidative stress in the ISs to overall oxidative stress in the retina.

In summary, we identified retinal lesions in normolipidemic and euglycemic *Cyp27a1*$^{-/-}$*Cyp46a1*$^{-/-}$ mice, and comprehensively characterized these animals to begin to elucidate the underlying reasons for the observed abnormalities. The data obtained point to the activation in the retina of vascular endothelium, monocytes/macrophages, and microglia cells because of intracellular cholesterol overload and impaired LXR signaling. These processes lead to oxidative stress and low-grade, persistent inflammation and cause vascular abnormalities. The key roles of LXRs as cholesterol and oxysterol sensors, which, in macrophages, help regulate the pathways of inflammation and immune response, suggest that agonists of these transcription factors should be considered for the treatment or prevention of retinal diseases characterized by vascular pathological conditions. Our findings highlight the metabolic and regulatory importance of enzymatic cholesterol elimination for normal status of retinal vasculature and establish retinal significance of this fundamental biological process. *Cyp27a1*$^{-/-}$*Cyp46a1*$^{-/-}$ mice could serve as a platform for pharmacological evaluation of LXR agonists and agents stimulating CYP46A1.

Acknowledgments

We thank Heather Butler and Kathryn Franke for mouse breeding, Dr. Ming-Jin Chang for animal genotyping, Cathy Doller for tissue sectioning, and Dr. Scott Howell for assistance with microscopy (all from the Visual Sciences Research Center Core Facility, Case Western Reserve University; Dr. Hisashi Fujioka (Case Western electron microscopy core facility) for help with electron microscopy; Dr. Alex Veenstra and Chieh Allen Lee for help with FA and hemoglobin A_{1c} measurements, respectively; and Jie Tang for retinal elastase digests.

Supplemental Data

Supplemental material for this article can be found at *http://dx.doi.org/10.1016/j.ajpath.2014.05.024*.

References

1. Fliesler SJ, Bretillon L: The ins and outs of cholesterol in the vertebrate retina. J Lipid Res 2010, 51:3399–3413
2. Pikuleva IA, Curcio CA: Cholesterol in the retina: the best is yet to come. Prog Retin Eye Res 2014, 41:64–89
3. Fliesler SJ, Florman R, Rapp LM, Pittler SJ, Keller RK: In vivo biosynthesis of cholesterol in the rat retina. FEBS Lett 1993, 335: 234–238
4. Elner VM: Retinal pigment epithelial acid lipase activity and lipoprotein receptors: effects of dietary omega-3 fatty acids. Trans Am Ophthalmol Soc 2002, 100:301–338
5. Tserentsoodol N, Sztein J, Campos M, Gordiyenko NV, Fariss RN, Lee JW, Fliesler SJ, Rodriguez IR: Uptake of cholesterol by the retina occurs primarily via a low density lipoprotein receptor-mediated process. Mol Vis 2006, 12:1306–1318
6. Lee JW, Fuda H, Javitt NB, Strott CA, Rodriguez IR: Expression and localization of sterol 27-hydroxylase (CYP27A1) in monkey retina. Exp Eye Res 2006, 83:465–469
7. Bretillon L, Diczfalusy U, Bjorkhem I, Maire MA, Martine L, Joffre C, Acar N, Bron A, Creuzot-Garcher C: Cholesterol-24S-hydroxylase (CYP46A1) is specifically expressed in neurons of the neural retina. Curr Eye Res 2007, 32:361–366
8. Liao WL, Heo GY, Dodder NG, Pikuleva IA, Turko IV: Optimizing the conditions of a multiple reaction monitoring assay for membrane proteins: quantification of cytochrome P450 11A1 and adrenodoxin reductase in bovine adrenal cortex and retina. Anal Chem 2010, 82: 5760–5767
9. Liao W-L, Heo GY, Dodder N, Reem R, Mast N, Huang C, DiPatre PL, Turko IV, Pikuleva IA: Quantification of cholesterol-metabolizing P450s CYP27A1 and CYP46A1 in neural tissues reveals a lack of enzyme-product correlations in human retina but not human brain. J Proteome Res 2011, 10:241–248
10. Mast N, Reem R, Bederman I, Huang S, DiPatre PL, Bjorkhem I, Pikuleva IA: Cholestenoic acid is an important elimination product of cholesterol in the retina: comparison of retinal cholesterol metabolism with that in the brain. Invest Ophthalmol Vis Sci 2011, 52:594–603
11. Wang M, Heo GY, Omarova S, Pikuleva IA, Turko IV: Sample prefractionation for mass spectrometry quantification of low-abundance membrane proteins. Anal Chem 2012, 84:5186–5191
12. Omarova S, Charvet CD, Reem RE, Mast N, Zheng W, Huang S, Peachey NS, Pikuleva IA: Abnormal vascularization in mouse retina with dysregulated retinal cholesterol homeostasis. J Clin Invest 2012, 122:3012–3023
13. Zheng W, Reem RE, Omarova S, Huang S, DiPatre PL, Charvet CD, Curcio CA, Pikuleva IA: Spatial distribution of the pathways of cholesterol homeostasis in human retina. PLoS One 2012, 7:e37926
14. Meaney S, Bodin K, Diczfalusy U, Bjorkhem I: On the rate of translocation in vitro and kinetics in vivo of the major oxysterols in human circulation: critical importance of the position of the oxygen function. J Lipid Res 2002, 43:2130–2135
15. Brown MS, Goldstein JL: Cholesterol feedback: from Schoenheimer's bottle to Scap's MELADL. J Lipid Res 2009, 50(Suppl):S15–S27
16. Janowski BA, Willy PJ, Devi TR, Falck JR, Mangelsdorf DJ: An oxysterol signalling pathway mediated by the nuclear receptor LXR alpha. Nature 1996, 383:728–731
17. Kalaany NY, Mangelsdorf DJ: LXRS and FXR: the yin and yang of cholesterol and fat metabolism. Annu Rev Physiol 2006, 68:159–191
18. Chen W, Chen G, Head DL, Mangelsdorf DJ, Russell DW: Enzymatic reduction of oxysterols impairs LXR signaling in cultured cells and the livers of mice. Cell Metab 2007, 5:73–79
19. Calkin AC, Tontonoz P: Transcriptional integration of metabolism by the nuclear sterol-activated receptors LXR and FXR. Nat Rev Mol Cell Biol 2012, 13:213–224
20. Korach-Andre M, Archer A, Gabbi C, Barros RP, Pedrelli M, Steffensen KR, Pettersson AT, Laurencikiene J, Parini P, Gustafsson JA: Liver X receptors regulate de novo lipogenesis in a tissue-specific manner in C57BL/6 female mice. Am J Physiol Endocrinol Metab 2011, 301:E210–E222
21. Pannu PS, Allahverdian S, Francis GA: Oxysterol generation and liver X receptor-dependent reverse cholesterol transport: not all roads lead to Rome. Mol Cell Endocrinol 2013, 368:99–107
22. Bjorkhem I: Five decades with oxysterols. Biochimie 2013, 95:448–454

23. Ramirez DM, Andersson S, Russell DW: Neuronal expression and subcellular localization of cholesterol 24-hydroxylase in the mouse brain. J Comp Neurol 2008, 507:1676–1693
24. Wikvall K: Hydroxylations in biosynthesis of bile acids: isolation of a cytochrome P-450 from rabbit liver mitochondria catalyzing 26-hydroxylation of C27-steroids. J Biol Chem 1984, 259:3800–3804
25. Reiss AB, Martin KO, Rojer DE, Iyer S, Grossi EA, Galloway AC, Javitt NB: Sterol 27-hydroxylase: expression in human arterial endothelium. J Lipid Res 1997, 38:1254–1260
26. Babiker A, Andersson O, Lund E, Xiu RJ, Deeb S, Reshef A, Leitersdorf E, Diczfalusy U, Bjorkhem I: Elimination of cholesterol in macrophages and endothelial cells by the sterol 27-hydroxylase mechanism: comparison with high density lipoprotein-mediated reverse cholesterol transport. J Biol Chem 1997, 272:26253–26261
27. Babiker A, Andersson O, Lindblom D, van der Linden J, Wiklund B, Lutjohann D, Diczfalusy U, Bjorkhem I: Elimination of cholesterol as cholestenoic acid in human lung by sterol 27-hydroxylase: evidence that most of this steroid in the circulation is of pulmonary origin. J Lipid Res 1999, 40:1417–1425
28. Lund EG, Guileyardo JM, Russell DW: cDNA cloning of cholesterol 24-hydroxylase, a mediator of cholesterol homeostasis in the brain. Proc Natl Acad Sci U S A 1999, 96:7238–7243
29. Dubrac S, Lear SR, Ananthanarayanan M, Balasubramaniyan N, Bollineni J, Shefer S, Hyogo H, Cohen DE, Blanche PJ, Krauss RM, Batta AK, Salen G, Suchy FJ, Maeda N, Erickson SK: Role of CYP27A in cholesterol and bile acid metabolism. J Lipid Res 2005, 46:76–85
30. Lund EG, Xie C, Kotti T, Turley SD, Dietschy JM, Russell DW: Knockout of the cholesterol 24-hydroxylase gene in mice reveals a brain-specific mechanism of cholesterol turnover. J Biol Chem 2003, 278:22980–22988
31. Charvet CD, Saadane A, Wang M, Salomon RG, Brunengraber H, Turko IV, Pikuleva IA: Pretreatment with pyridoxamine mitigates isolevuglandin-associated retinal effects in mice exposed to bright light. J Biol Chem 2013, 288:29267–29280
32. Veenstra AA, Tang J, Kern TS: Antagonism of CD11b with neutrophil inhibitory factor (NIF) inhibits vascular lesions in diabetic retinopathy. PLoS One 2013, 8:e78405
33. Daugherty A, Whitman SC: Quantification of atherosclerosis in mice. Methods Mol Biol 2003, 209:293–309
34. Mast N, Shafaati M, Zaman W, Zheng W, Prusak D, Wood T, Ansari GA, Lovgren-Sandblom A, Olin M, Bjorkhem I, Pikuleva I: Marked variability in hepatic expression of cytochromes CYP7A1 and CYP27A1 as compared to cerebral CYP46A1: lessons from a dietary study with omega 3 fatty acids in hamsters. Biochim Biophys Acta 2010, 1801:674–681
35. Lund E, Sisfontes L, Reihner E, Bjorkhem I: Determination of serum levels of unesterified lathosterol by isotope dilution-mass spectrometry. Scand J Clin Lab Invest 1989, 49:165–171
36. Bjorkhem I, Hansson M: Cerebrotendinous xanthomatosis: an inborn error in bile acid synthesis with defined mutations but still a challenge. Biochem Biophys Res Commun 2010, 396:46–49
37. Bavner A, Shafaati M, Hansson M, Olin M, Shpitzen S, Meiner V, Leitersdorf E, Bjorkhem I: On the mechanism of accumulation of cholestanol in the brain of mice with a disruption of sterol 27-hydroxylase. J Lipid Res 2010, 51:2722–2730
38. Castanho MA, Coutinho A, Prieto MJ: Absorption and fluorescence spectra of polyene antibiotics in the presence of cholesterol. J Biol Chem 1992, 267:204–209
39. Fliesler SJ, Schroepfer GJ Jr: Sterol composition of bovine retinal rod outer segment membranes and whole retinas. Biochim Biophys Acta 1982, 711:138–148
40. Bhattacharyya AK, Lin DS, Connor WE: Cholestanol metabolism in patients with cerebrotendinous xanthomatosis: absorption, turnover, and tissue deposition. J Lipid Res 2007, 48:185–192
41. Suter M, Reme C, Grimm C, Wenzel A, Jaattela M, Esser P, Kociok N, Leist M, Richter C: Age-related macular degeneration: the lipofusion component N-retinyl-N-retinylidene ethanolamine detaches proapoptotic proteins from mitochondria and induces apoptosis in mammalian retinal pigment epithelial cells. J Biol Chem 2000, 275:39625–39630
42. Finnemann SC, Leung LW, Rodriguez-Boulan E: The lipofuscin component A2E selectively inhibits phagolysosomal degradation of photoreceptor phospholipid by the retinal pigment epithelium. Proc Natl Acad Sci U S A 2002, 99:3842–3847
43. Buhman KK, Chen HC, Farese RV Jr: The enzymes of neutral lipid synthesis. J Biol Chem 2001, 276:40369–40372
44. Okuda A, Okuda K: Purification and characterization of delta 4-3-ketosteroid 5 beta-reductase. J Biol Chem 1984, 259:7519–7524
45. Tani T, Ohsumi J, Mita K, Takiguchi Y: Identification of a novel class of elastase isozyme, human pancreatic elastase III, by cDNA and genomic gene cloning. J Biol Chem 1988, 263:1231–1239
46. Jaffray C, Yang J, Carter G, Mendez C, Norman J: Pancreatic elastase activates pulmonary nuclear factor kappa B and inhibitory kappa B, mimicking pancreatitis-associated adult respiratory distress syndrome. Surgery 2000, 128:225–231
47. Sziegoleit A, Linder D, Schluter M, Ogawa M, Nishibe S, Fujimoto K: Studies on the specificity of the cholesterol-binding pancreatic proteinase and identification as human pancreatic elastase 1. Eur J Biochem 1985, 151:595–599
48. Mattapallil MJ, Wawrousek EF, Chan CC, Zhao H, Roychoudhury J, Ferguson TA, Caspi RR: The Rd8 mutation of the Crb1 gene is present in vendor lines of C57BL/6N mice and embryonic stem cells, and confounds ocular induced mutant phenotypes. Invest Ophthalmol Vis Sci 2012, 53:2921–2927
49. Chang B, Hurd R, Wang J, Nishina P: Survey of common eye diseases in laboratory mouse strains. Invest Ophthalmol Vis Sci 2013, 54:4974–4981
50. Chang B, Hawes NL, Hurd RE, Davisson MT, Nusinowitz S, Heckenlively JR: Retinal degeneration mutants in the mouse. Vision Res 2002, 42:517–525
51. Mehalow AK, Kameya S, Smith RS, Hawes NL, Denegre JM, Young JA, Bechtold L, Haider NB, Tepass U, Heckenlively JR, Chang B, Naggert JK, Nishina PM: CRB1 is essential for external limiting membrane integrity and photoreceptor morphogenesis in the mammalian retina. Hum Mol Genet 2003, 12:2179–2189
52. Chu XK, Wang Y, Ardeljan D, Tuo J, Chan CC: Controversial view of a genetically altered mouse model of focal retinal degeneration. Bioengineered 2013, 4:130–135
53. Querques G, Avellis FO, Querques L, Massamba N, Bandello F, Souied EH: Three dimensional spectral domain optical coherence tomography features of retinal-choroidal anastomosis. Graefes Arch Clin Exp Ophthalmol 2012, 250:165–173
54. Curtis TM, Gardiner TA, Stitt AW: Microvascular lesions of diabetic retinopathy: clues towards understanding pathogenesis? Eye (Lond) 2009, 23:1496–1508
55. Tang J, Kern TS: Inflammation in diabetic retinopathy. Prog Retin Eye Res 2011, 30:343–358
56. Yannuzzi LA, Freund KB, Takahashi BS: Review of retinal angiomatous proliferation or type 3 neovascularization. Retina 2008, 28:375–384
57. Villacampa N, Almolda B, Gonzalez B, Castellano B: Tomato lectin histochemistry for microglial visualization. Methods Mol Biol 2013, 1041:261–279
58. Jimeno D, Velasco A, Lillo C, Lara JM, Aijon J: Response of microglial cells after a cryolesion in the peripheral proliferative retina of tench. Brain Res 1999, 816:175–189
59. Stoeckenius W: [Osmium tetroxide staining of intracellular myelin patterns] German. Exp Cell Res 1957, 13:410–414
60. Zelcer N, Tontonoz P: Liver X receptors as integrators of metabolic and inflammatory signaling. J Clin Invest 2006, 116:607–614
61. Santos AM, Calvente R, Tassi M, Carrasco MC, Martin-Oliva D, Marin-Teva JL, Navascues J, Cuadros MA: Embryonic and postnatal development of microglial cells in the mouse retina. J Comp Neurol 2008, 506:224–239

62. Hynes RO: Integrins: bidirectional, allosteric signaling machines. Cell 2002, 110:673–687
63. Coxon A, Rieu P, Barkalow FJ, Askari S, Sharpe AH, von Andrian UH, Arnaout MA, Mayadas TN: A novel role for the beta 2 integrin CD11b/CD18 in neutrophil apoptosis: a homeostatic mechanism in inflammation. Immunity 1996, 5:653–666
64. Damerau B, Grunefeld E, Vogt W: Chemotactic effects of the complement-derived peptides C3a, C3ai and C5a (classical anaphylatoxin) on rabbit and guinea-pig polymorphonuclear leukocytes. Naunyn Schmiedebergs Arch Pharmacol 1978, 305:181–184
65. Cashman SM, Desai A, Ramo K, Kumar-Singh R: Expression of complement component 3 (C3) from an adenovirus leads to pathology in the murine retina. Invest Ophthalmol Vis Sci 2011, 52:3436–3445
66. Tegla CA, Cudrici C, Patel S, Trippe R 3rd, Rus V, Niculescu F, Rus H: Membrane attack by complement: the assembly and biology of terminal complement complexes. Immunol Res 2011, 51:45–60
67. Kuzmanovic M, Dudley VJ, Sarthy VP: GFAP promoter drives Muller cell-specific expression in transgenic mice. Invest Ophthalmol Vis Sci 2003, 44:3606–3613
68. Ekstrom P, Sanyal S, Narfstrom K, Chader GJ, van Veen T: Accumulation of glial fibrillary acidic protein in Muller radial glia during retinal degeneration. Invest Ophthalmol Vis Sci 1988, 29:1363–1371
69. Wu KH, Madigan MC, Billson FA, Penfold PL: Differential expression of GFAP in early v late AMD: a quantitative analysis. Br J Ophthalmol 2003, 87:1159–1166
70. Hopkins PN: Molecular biology of atherosclerosis. Physiol Rev 2013, 93:1317–1542
71. Salomon RG, Miller DB: Levuglandins: isolation, characterization, and total synthesis of new secoprostanoid products from prostaglandin endoperoxides. Adv Prostaglandin Thromboxane Leukot Res 1985, 15:323–326
72. Smith LL: Review of progress in sterol oxidations: 1987-1995. Lipids 1996, 31:453–487
73. Salomon RG, Subbanagounder G, O'Neil J, Kaur K, Smith MA, Hoff HF, Perry G, Monnier VM: Levuglandin E2-protein adducts in human plasma and vasculature. Chem Res Toxicol 1997, 10:536–545
74. Li W, Laird JM, Lu L, Roychowdhury S, Nagy LE, Zhou R, Crabb JW, Salomon RG: Isolevuglandins covalently modify phosphatidylethanolamines in vivo: detection and quantitative analysis of hydroxylactam adducts. Free Radic Biol Med 2009, 47:1539–1552
75. Amaral J, Lee JW, Chou J, Campos MM, Rodriguez IR: 7-Ketocholesterol induces inflammation and angiogenesis in vivo: a novel rat model. PLoS One 2013, 8:e56099
76. Salomon RG, Subbanagounder G, Singh U, O'Neil J, Hoff HF: Oxidation of low-density lipoproteins produces levuglandin-protein adducts. Chem Res Toxicol 1997, 10:750–759
77. Hoppe G, Subbanagounder G, O'Neil J, Salomon RG, Hoff HF: Macrophage recognition of LDL modified by levuglandin E2, an oxidation product of arachidonic acid. Biochim Biophys Acta 1997, 1344:1–5
78. Salen G: Cholestanol deposition in cerebrotendinous xanthomatosis: a possible mechanism. Ann Intern Med 1971, 75:843–851
79. Skrede S, Bjorkhem I, Buchmann MS, Hopen G, Fausa O: A novel pathway for biosynthesis of cholestanol with 7 alpha-hydroxylated C27-steroids as intermediates, and its importance for the accumulation of cholestanol in cerebrotendinous xanthomatosis. J Clin Invest 1985, 75:448–455
80. Moore KJ, Tabas I: Macrophages in the pathogenesis of atherosclerosis. Cell 2011, 145:341–355
81. Carr MW, Roth SJ, Luther E, Rose SS, Springer TA: Monocyte chemoattractant protein 1 acts as a T-lymphocyte chemoattractant. Proc Natl Acad Sci U S A 1994, 91:3652–3656
82. Bensinger SJ, Bradley MN, Joseph SB, Zelcer N, Janssen EM, Hausner MA, Shih R, Parks JS, Edwards PA, Jamieson BD, Tontonoz P: LXR signaling couples sterol metabolism to proliferation in the acquired immune response. Cell 2008, 134:97–111
83. Ghisletti S, Huang W, Ogawa S, Pascual G, Lin ME, Willson TM, Rosenfeld MG, Glass CK: Parallel SUMOylation-dependent pathways mediate gene- and signal-specific transrepression by LXRs and PPARgamma. Mol Cell 2007, 25:57–70
84. Wolpe SD, Sherry B, Juers D, Davatelis G, Yurt RW, Cerami A: Identification and characterization of macrophage inflammatory protein 2. Proc Natl Acad Sci U S A 1989, 86:612–616
85. Beutler B, Greenwald D, Hulmes JD, Chang M, Pan YC, Mathison J, Ulevitch R, Cerami A: Identity of tumour necrosis factor and the macrophage-secreted factor cachectin. Nature 1985, 316:552–554
86. Yates JR, Sepp T, Matharu BK, Khan JC, Thurlby DA, Shahid H, Clayton DG, Hayward C, Morgan J, Wright AF, Armbrecht AM, Dhillon B, Deary IJ, Redmond E, Bird AC, Moore AT: Complement C3 variant and the risk of age-related macular degeneration. N Engl J Med 2007, 357:553–561
87. Zhang J, Gerhardinger C, Lorenzi M: Early complement activation and decreased levels of glycosylphosphatidylinositol-anchored complement inhibitors in human and experimental diabetic retinopathy. Diabetes 2002, 51:3499–3504
88. Sene A, Khan AA, Cox D, Nakamura RE, Santeford A, Kim BM, Sidhu R, Onken MD, Harbour JW, Hagbi-Levi S, Chowers I, Edwards PA, Baldan A, Parks JS, Ory DS, Apte RS: Impaired cholesterol efflux in senescent macrophages promotes age-related macular degeneration. Cell Metab 2013, 17:549–561
89. Hazra S, Rasheed A, Bhatwadekar A, Wang X, Shaw LC, Patel M, Caballero S, Magomedova L, Solis N, Yan Y, Wang W, Thinschmidt JS, Verma A, Li Q, Levi M, Cummins CL, Grant MB: Liver X receptor modulates diabetic retinopathy outcome in a mouse model of streptozotocin-induced diabetes. Diabetes 2012, 61:3270–3279
90. Mast N, Li Y, Linger M, Clark M, Wiseman J, Pikuleva IA: Pharmacologic stimulation of cytochrome P450 46A1 and cerebral cholesterol turnover in mice. J Biol Chem 2014, 289:3529–3538
91. Du Y, Veenstra A, Palczewski K, Kern TS: Photoreceptor cells are major contributors to diabetes-induced oxidative stress and local inflammation in the retina. Proc Natl Acad Sci U S A 2013, 110:16586–16591
92. Kennedy MA, Barrera GC, Nakamura K, Baldan A, Tarr P, Fishbein MC, Frank J, Francone OL, Edwards PA: ABCG1 has a critical role in mediating cholesterol efflux to HDL and preventing cellular lipid accumulation. Cell Metab 2005, 1:121–131
93. Sturek JM, Castle JD, Trace AP, Page LC, Castle AM, Evans-Molina C, Parks JS, Mirmira RG, Hedrick CC: An intracellular role for ABCG1-mediated cholesterol transport in the regulated secretory pathway of mouse pancreatic beta cells. J Clin Invest 2010, 120:2575–2589
94. Baldan A, Tarr P, Vales CS, Frank J, Shimotake TK, Hawgood S, Edwards PA: Deletion of the transmembrane transporter ABCG1 results in progressive pulmonary lipidosis. J Biol Chem 2006, 281:29401–29410
95. Wojcik AJ, Skaflen MD, Srinivasan S, Hedrick CC: A critical role for ABCG1 in macrophage inflammation and lung homeostasis. J Immunol 2008, 180:4273–4282
96. Kalaany NY, Gauthier KC, Zavacki AM, Mammen PP, Kitazume T, Peterson JA, Horton JD, Garry DJ, Bianco AC, Mangelsdorf DJ: LXRs regulate the balance between fat storage and oxidation. Cell Metab 2005, 1:231–244
97. Patel R, Patel M, Tsai R, Lin V, Bookout AL, Zhang Y, Magomedova L, Li T, Chan JF, Budd C, Mangelsdorf DJ, Cummins CL: LXRbeta is required for glucocorticoid-induced hyperglycemia and hepatosteatosis in mice. J Clin Invest 2011, 121:431–441
98. Schuster GU, Parini P, Wang L, Alberti S, Steffensen KR, Hansson GK, Angelin B, Gustafsson JA: Accumulation of foam cells in liver X receptor-deficient mice. Circulation 2002, 106:1147–1153